Complex Formation of Ni^{II}, Cu^{II}, Pd^{II}, and Co^{III} with 1,2,3,4-Tetraaminobutane**

Anja Zimmer,[a] Dirk Kuppert,[a] Thomas Weyhermüller,[b] Iris Müller,[c] and Kaspar Hegetschweiler*[a]

Abstract: Complex formation of the two tetraamine ligands (2*S*,3*S*)-1,2,3,4-tetraaminobutane (*threo*-tetraaminobutane, *t*tab) and (2*R*,3*S*)-1,2,3,4-tetraaminobutane (*erythro*-tetraaminobutane, *e*tab) with Co^{III}, Ni^{II}, Cu^{II}, and Pd^{II} was investigated in aqueous solution and in the solid state. For Ni^{II} and Cu^{II}, the pH-dependent formation of a variety of species $[M^{II}_xL_yH_z]^{(2x+z)+}$ was established by potentiometric titrations and UV/Vis spectroscopy. In sufficiently acidic solutions the divalent cations formed a mononuclear complex with the doubly protonated ligand of composition $[M(H_2L)]^{4+}$. An example of such a complex was characterized in the crystal structure of $[Pd(H_2ttab)Cl_2]Cl_2 \cdot H_2O$. If the metal cation was present in excess, increase of pH resulted in the formation of dinuclear complexes $[M_2L]^{4+}$. Such a species was found in the crystal structure of $[Cu_2(ttab)Br_4] \cdot H_2O$. Excess ligand, on the other hand, lead to the formation of a series of mononuclear bis-complexes $[M^q(H_xL)(H_yL)]^{(q+x+y)+}$. The crystal structure of $[Co(Hetab)_2][ZnCl_4]_2Cl \cdot H_2O$ with the inert, trivalent Co^{III} center served as a model to illustrate the structural features of this class of complexes. By using an approximately equimolar ratio of the ligand and the metal cation, a variety of polymeric aggregates both in dilute aqueous solution and in the solid state were observed. The crystal structure of $Cu_2(ttab)_3Br_4$, which exhibits a two-dimensional, infinite network, and that of $[Ni_8(ttab)_{12}]Br_{16} \cdot 17.5\,H_2O$, which contains discrete chiral $[Ni_8(ttab)_{12}]^{16+}$ cubes with approximate *T* symmetry, are representative examples of such polymers. The energy of different diastereomeric forms of such complexes with the two tetraamine ligands were analyzed by means of molecular mechanics calculations, and the implications of these calculations for the different structures are discussed.

Keywords: coordination polymers · copper · nickel · polyamines · supramolecular chemistry

Introduction

The design of extended molecular networks is an important field in modern chemistry and has been discussed extensively in terms of crystal engineering, self-assembly processes, and supramolecular chemistry.[1, 2] The two most important types of molecular interactions that have been utilized for the construction of extended molecular architectures are hydrogen bonding[3] and multiple binding of metal cations to suitable ligands[4, 5] (formation of coordination polymers). The design of chiral structures is of particular importance, because a variety of interesting chemical and physical properties, such as enantioselective catalytic activity, specific binding of chiral guests, electrical and optical properties, depend upon crystal polarity or chirality.[6, 7]

The use of specific chiral receptors for metal ions as molecular building blocks would be a straightforward strategy for the design of chiral polymers. However, it seems that this approach has not been exploited systematically to any large extent.[7] Linear primary polyamines of composition $H_2N{-}CH_2{-}(CH{-}NH_2)_n{-}CH_2{-}NH_2$ with more than three

[a] Prof. K. Hegetschweiler, Dipl.-Chem. A. Zimmer, Dr. D. Kuppert
Anorganische Chemie, Universität des Saarlandes
66041 Saarbrücken (Germany)
Fax: (+49) 681-302-2663
E-mail: hegetschweiler@mx.uni-saarland.de

[b] Dr. T. Weyhermüller
Max-Planck-Institut für Strahlenchemie
Stiftstrasse 34-36, 45470 Mülheim an der Ruhr (Germany)

[c] Dr. I. Müller
Analytische Chemie, Ruhr-Universität
Universitätsstrasse 150, 44780 Bochum (Germany)

[**] Linear Primary Polyamines as Building Blocks for Coordination Polymers, Part 3; for Part 2 see: ref. [9].

Supporting information for this article is available on the WWW under http://www.wiley-vch.de/home/chemistry/ or from the author. Table S1 lists UV/Vis data and corresponding references for the Ni^{II} and Cu^{II} amine complexes in aqueous solution used for Figure 9. Table S2 and S3 list experimental data for the potentiometric titrations. Figures S1, S2, S3, S4, and S5 show additional structural features of $[Co(Hetab)_2][ZnCl_4]_2Cl \cdot H_2O$, $[Pd(H_2ttab)Cl_2]Cl_2 \cdot H_2O$, $[Cu_2(ttab)Br_4] \cdot H_2O$, $Cu_2(ttab)_3Br_4$, and $[Ni_8(ttab)_{12}]Br_{16} \cdot 17.5\,H_2O$. Figures S6, S7, and S8 show species distribution diagrams of the Cu^{II}-*e*tab, Ni^{II}-*t*tab, and Ni^{II}-*e*tab system, and Figure S9 shows spectral changes for the Cu-*t*tab system during a titration experiment with excess ligand.

  0947-6539/01/0704-0917 $ 17.50+.50/0

NH_2 groups ($n \geqslant 2$) are potentially chiral, and steric constraints dictate that these ligands cannot coordinate the entire donor set to a single metal cation. These compounds thus have the ideal prerequisites to serve as specific molecular building blocks for chiral coordination polymers. In a previous contribution we reported a facile synthetic route to such polyamines.[8] The amines can be prepared readily from the corresponding polyalcohols (sugar alcohols), which represent a rich, easily accessible, and inexpensive reservoir of chiral and optically pure starting materials. Furthermore it has been demonstrated that this conversion is completely stereo specific.[8, 9] We have undertaken a comprehensive study of the coordination chemistry of these compounds and we report here on the solid-state structures of Co^{III}, Ni^{II}, Cu^{II}, and Pd^{II} complexes with the *erythro*- and the chiral *threo*-isomers of 1,2,3,4-tetraaminobutane (*e*tab and *t*tab, respectively). In addition, we have established the species composition and stability constants of Cu^{II} and Ni^{II} complexes with these two isomers in dilute aqueous solution.

Results

Preparation and structural characterization of solid compounds: Single crystals of composition $[Co(Hetab)_2][ZnCl_4]_2 \cdot Cl \cdot H_2O$, $[Pd(H_2ttab)Cl_2]Cl_2 \cdot H_2O$, $Cu_2(ttab)_3Br_4$, $[Cu_2(ttab)Br_4] \cdot H_2O$, and $[Ni_8(ttab)_{12}]Br_{16} \cdot 17.5\,H_2O$ were all grown from aqueous solution and characterized by X-ray diffraction. Views of their molecular structures are depicted in Figures 1–5, and graphical illustrations of the packing are provided as Supporting Information.

$[Co(Hetab)_2]^{5+}$ was prepared by the usual aerial oxidation of the corresponding Co^{II} precursor in aqueous solution with charcoal as catalyst; it was isolated as a chloride salt. The ^{13}C NMR spectrum (16 major and several minor signals) indicated the presence of a variety of diastereomeric complexes with Co^{III}–hexaamine coordination (UV/Vis: λ_{max} at 329 and 459 nm).[10] Two different tridentate coordination modes of this ligand must be taken into account (Scheme 1a): coordination through N(1), N(2), and N(3) [(1,2,3)-mode] giving one six-membered and two five-membered chelate rings, and coordination through N(1), N(2), and N(4) [(1,2,4)-mode] giving one seven-, one six-, and one five-membered chelate ring. The combination of these modes generates three different types of molecular structure: a bis-(1,2,3), a mixed (1,2,3)-(1,2,4) and a bis-(1,2,4) structure. For each of the three structures a variety of diastereomers must be considered. The total number of possible diastereomers can be elucidated by following the schematic representation shown in Scheme 1b: The three coordinated nitrogen atoms of a ligand are labeled as N(A), N(B), and N(C) with N(A) = N(1). Two such donor sets define a trigonal CoN_6 antiprism. The complex is now viewed along the pseudo-threefold axis of this antiprism, and the donor set of the upper ligand is wound clockwise in the order A-B-C and held fixed for the following considerations. In the structures **1**–**3**, the lower ligand also has a clockwise orientation. If the two nitrogen atoms N(A) and N(A′) of the two ligands are placed in *cis* positions, the other nitrogen atoms N(B)/N(B′) and N(C)/N(C′) will also be positioned

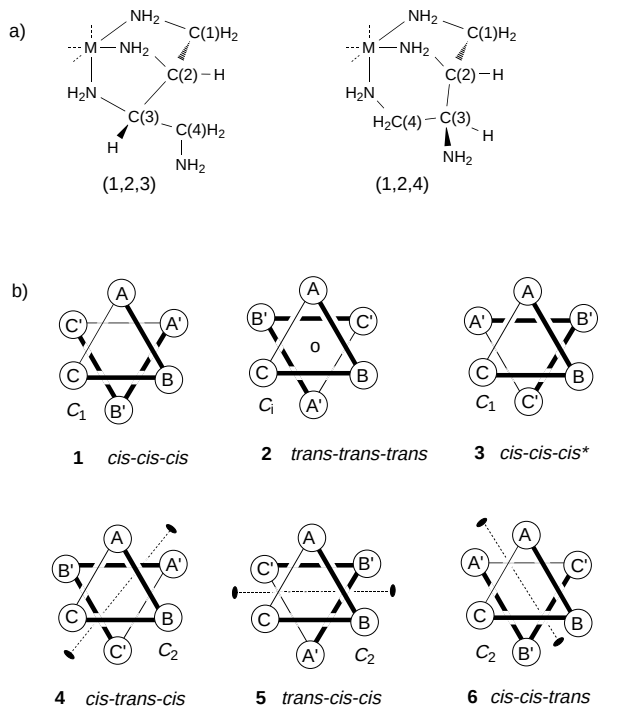

Scheme 1. The different isomers of a hexaamine $[M^z(etab)_2]^{z+}$ complex. a) The two possible structures (1,2,3) and (1,2,4) for a tridentate coordination of the ligand. b) View along the pseudo threefold axis of the MN_6 antiprism formed by the two donor sets of the bis-complex. N(1) = A, N(2) = B and N(3) = C for the (1,2,3)-coordination and N(1) = A, N(2) = B, N(4) = C for the (1,2,4)-coordination. The stereo descriptors refer to the positions of related atoms in the two ligands (A-A′, B-B′, C-C′). The symmetry labels (C_1, C_i, C_2) and the symmetry elements (center of inversion and twofold axis) refer to either a bis-(1,2,3) or a bis-(1,2,4) complex. The six diastereomers with a (1,2,3)-(1,2,4)-structure are all completely asymmetric (C_1).

cis to each other; the resulting species (**1**) is labeled as the *cis-cis-cis* isomer. Clockwise rotation of the lower ligand by 120° generates the *trans-trans-trans* form (**2**). Further rotation generates another *cis-cis-cis* form (**3**). In representation **4**, the lower ligand is wound anti-clockwise and the two nitrogens N(A) and N(A′) are again placed in *cis* to each other. Two rotations by 120° give the two additional forms **5** and **6**. For the bis-(1,2,3)-structure, the two ligands have the same coordination with N(B) = N(2) and N(C) = N(3). In this case representation **3** is the mirror image of **1** and consequently a total of five different diastereomers must be accounted for. These diastereomers have C_1 (**1**), C_i (**2**) or C_2 (**4**–**6**) symmetry. Exactly the same considerations are valid for the bis-(1,2,4) structure with the assignment N(B) = N(2) and N(C) = N(4), that is, five diastereomers are possible. For the mixed (1,2,3)-(1,2,4)-mode, the two ligands are inequivalent and, consequently, the representations **1** and **3** refer to different diastereomers. This gives six additional, completely asymmetric (C_1) isomers. Altogether, there is a total of 16 possible isomers for $[Co^{III}(Hetab)_2]^{5+}$. Separation of different components by chromatographic procedures (Sephadex) was not successful, however, it was possible to crystallize one of the main species as $[Co(Hetab)_2][ZnCl_4]_2Cl \cdot H_2O$. Single-crystal X-ray analysis showed the presence of two crystallographically independent $[Co(Hetab)_2]^{5+}$ cations in this structure (Figure 1), both with a *trans-trans-trans* (**2**) bis-(1,2,3)-

0947-6539/01/0704-0918 $ 17.50+.50/0 *Chem. Eur. J.* **2001**, *7*, No. 4

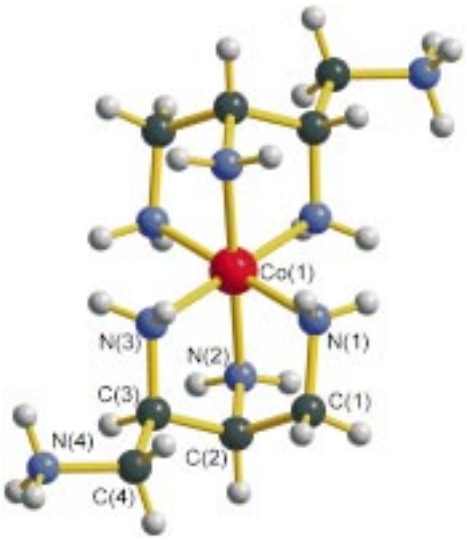

Figure 1. Ball and stick model of one of the $[Co(Hetab)_2]^{5+}$ cations with numbering scheme. Selected bond lengths [Å] and angles [°]: Co(1)–N(1) 1.956(7), Co(1)–N(2) 1.949(7), Co(1)–N(3) 1.974(7), N(1)-Co(1)-N(2) 83.2(3), N(1)-Co(1)-N(3) 84.8(3), N(1)-Co(1)-N(1A) 180.0, N(1)-Co(1)-N(2A) 96.8(3), N(1)-Co(1)-N(3A) 95.2(3), N(2)-Co(1)-N(3) 85.6(3), N(2)-Co(1)-N(2A) 180.0, N(2)-Co(1)-N(3A) 94.4(3), N(3)-Co(1)-N(3A) 180.0.

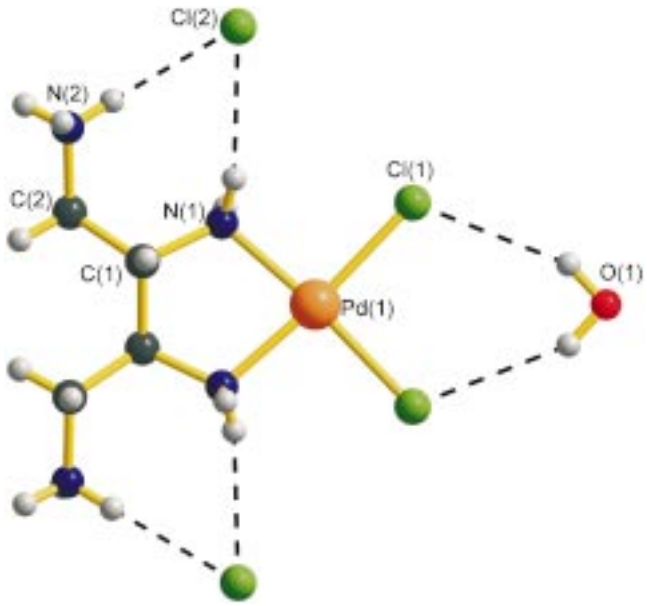

Figure 2. Molecular structure of $[Pd(H_2ttab)Cl_2]Cl_2 \cdot H_2O$ (ball and stick model). Selected bond lengths [Å] and angles [°]: Pd–N(1) 2.025(2), Pd–Cl(1) 2.3022(6), N(1)–C(1) 1.483(4), C(1)–C(2) 1.506(4), C(1)–C(1A) 1.536(5), N(2)–C(2) 1.483(4), N(1)-Pd(1)-N(1A) 83.0(1), N(1)-Pd(1)-Cl(1) 91.97(7), N(1)-Pd(1)-Cl(1A) 174.81(9), Cl(1)-Pd(1)-Cl(1A) 93.11(3).

geometry. In accordance with the assigned C_i symmetry both Co^{III} centers are located on centers of inversion. Although the two cations are crystallographically inequivalent, their molecular geometry does not differ significantly.

The crystal structure of $[Co(Hetab)_2][ZnCl_4]_2Cl \cdot H_2O$ can be described in terms of an extended, infinite, three-dimensional framework of hydrogen bonds. The $[Zn(1)Cl_4]^{2-}$ counter ions, the water molecules, and the non-coordinating, protonated nitrogen atoms of the complex cations are arranged into chains along the crystallographic *a* axis. These chains are interlinked by interactions between $[Zn(2)Cl_4]^{2-}$ anions and N–H groups of coordinated nitrogen donors generating additional chains along the *b* axis. Further interactions between coordinated N-H groups and Cl^- counter ions form chains along the *c* axis. Views of this hydrogen-bonded chain structure are shown in Figure S1 (see the Supporting Information).

As in $[Co(Hetab)_2]^{5+}$, the Pd^{II} complex $[Pd(H_2ttab)Cl_2]^{2+}$ is mononuclear and contains a partially protonated ligand (Figure 2). This complex was obtained from an acidic aqueous solution by the reaction $PdCl_2(s) + ttab \cdot 4HCl \rightarrow [Pd(H_2ttab)Cl_2]Cl_2 + 2HCl$. Evidently, protonation of the two non-coordinated amino groups prevents further binding interactions of the ligand to additional Pd centers. The complex cations are located on crystallographic twofold axes (C_2 point symmetry), and exhibit the expected square-planar *cis*-PdN_2Cl_2 geometry (Figure 2). They are stacked along the *c* axis with a Pd···Pd separation of 3.39 Å (Figure S2, Supporting Information). Such weak Pd–Pd interactions are well established for square-planar Pd^{II} complexes in the solid state.[11] In agreement with simple electrostatic considerations the two protons are bound to the two terminal amino groups and the Pd center is coordinated to N(2) and N(3) (labeled as (2,3)-coordination), forming a five-membered chelate ring.

The complex $[Cu_2(ttab)Br_4] \cdot H_2O$ has a polymeric structure (Figure 3). As already indicated by its stoichiometry, each ligand molecule binds two Cu^{II} cations, forming a chiral, C_2-symmetric $[Cu_2L]^{4+}$ moiety. This binding mode is labeled as (1,2)-(3,4). The two Cu^{II} centers, which are each additionally bonded to two Br^- ligands, have a distorted square-planar coordination environment (Cu–Br bond length: 2.41 Å). The Cu^{II} centers are also connected through a weak binding interaction to a Br^- ligand of a neighboring $\{Br_2CuLCuBr_2\}$ entity. The length of this Cu···Br interaction is 2.94 Å, which is significantly shorter than the sum of the van der Waals radii (3.8 Å);[12] also the Cu^{II} center is slightly displaced out of the mean N_2Br_2 plane by 0.17 Å towards the bridging Br^- ligand. The entire coordination sphere of Cu^{II} can thus be described as a square pyramid, with the loosely bonded Br^- in the apex. The two types of linking interactions, that is, the Br–Cu···Br and the Cu-L-Cu bridges give rise to a three-dimensional porous architecture. Five different types of structural motifs can be recognized in this network.

1) Cu–Br···Cu–Br···Cu–Br zigzag chains arranged parallel to either the *a* or *b* axis of the tetragonal crystal system. The chains are aligned parallel to each other and form $CuBr_2$ layers parallel to the *ab* plane, with an inter-chain Br···Br distance of 3.82 Å (corresponding to twice the van der Waals radius of Br).[12]

2) The $CuBr_2$ layers are interconnected by the bridging tetraamine ligands that form an alternating stack of purely "inorganic" ($CuBr_2$) and "organic" (L, H_2O) domains along the *c* axis.

3) Cu-L-Cu-Br···Cu-L-Cu-Br chains wind around the principal crystallographic 4_1 axes to form a helix.

4) Large Cu-Br···Cu-L-Cu-Br···Cu-L-Cu-Br···Cu-Br··· Cu-L-Cu-Br···Cu-L-Cu-Br cycles composed of a total of ten

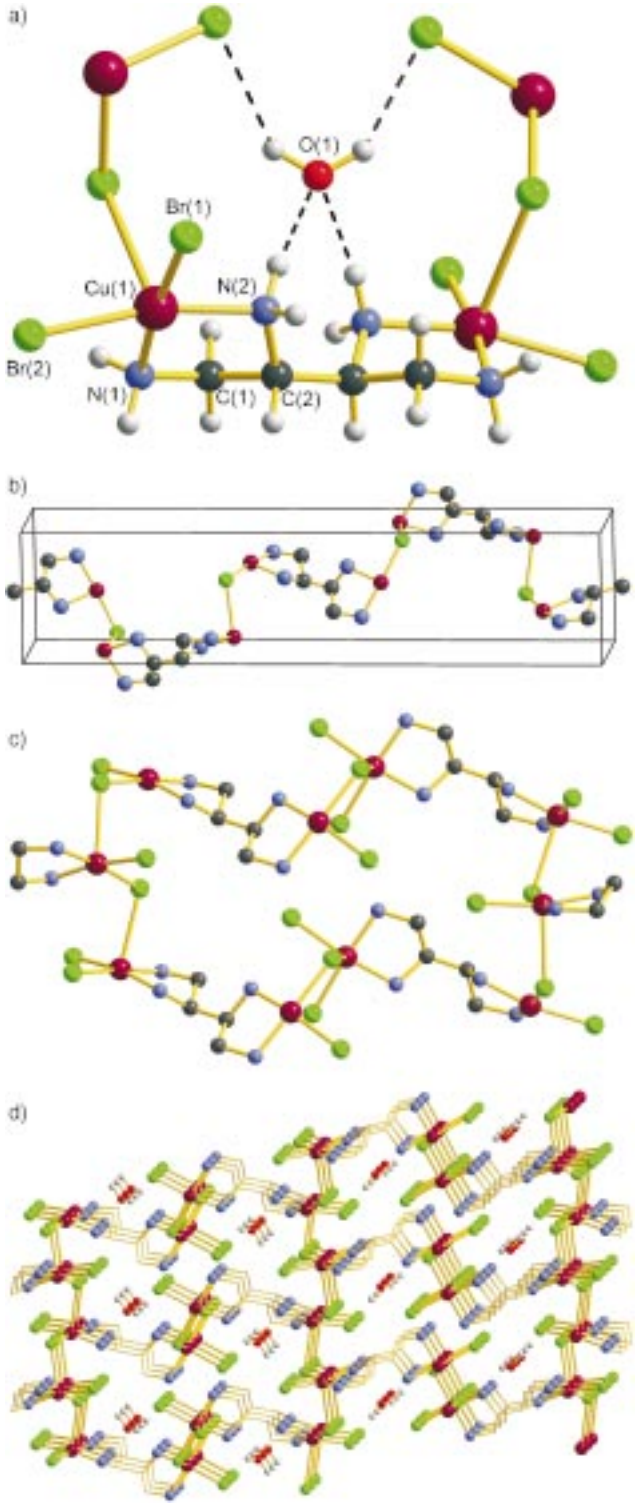

Figure 3. Crystal structure of $[Cu_2(ttab)Br_4]\cdot H_2O$ (ball and stick model). a) The $[Br_2Cu\text{-}L\text{-}CuBr_2]\cdot H_2O$ unit together with two adjacent $CuBr_2$ moieties; b) the Cu-L-Cu-Br helix; c) the $Cu_{10}\text{-}Br_6\text{-}L_4$ ring structure; d) a view of the entire packing. Selected bond lengths [Å]: Cu–N(1) 2.023(6), Cu–N(2) 2.014(6), Cu–Br(1) 2.414(1), Cu–Br(2) 2.412(1).

Cu atoms are formed. These rings are a result of the cross-linking between the helices and the inorganic Cu-Br···Cu chains.

5) A system of channels are formed that are arranged parallel to the *a* and *b* axes. The channels are generated by the stacking of the Cu_{10} rings and are filled with water molecules. Each water molecule is hydrogen bonded by two donating O–H···Br interactions involving the non-bridging Br^- ligands of the Cu–Br···Cu chains and by two accepting N–H···O bonds from the two amino groups in the 2- and 3-position of the tetraamine ligand.

In contrast to $[Cu_2(ttab)Br_4]\cdot H_2O$ for which the Cu:L ratio is 2:1, the complex $Cu_2(ttab)_3Br_4$ contains a 1.5-fold excess of the ligand (Figure 4). Both compounds have the same C_2

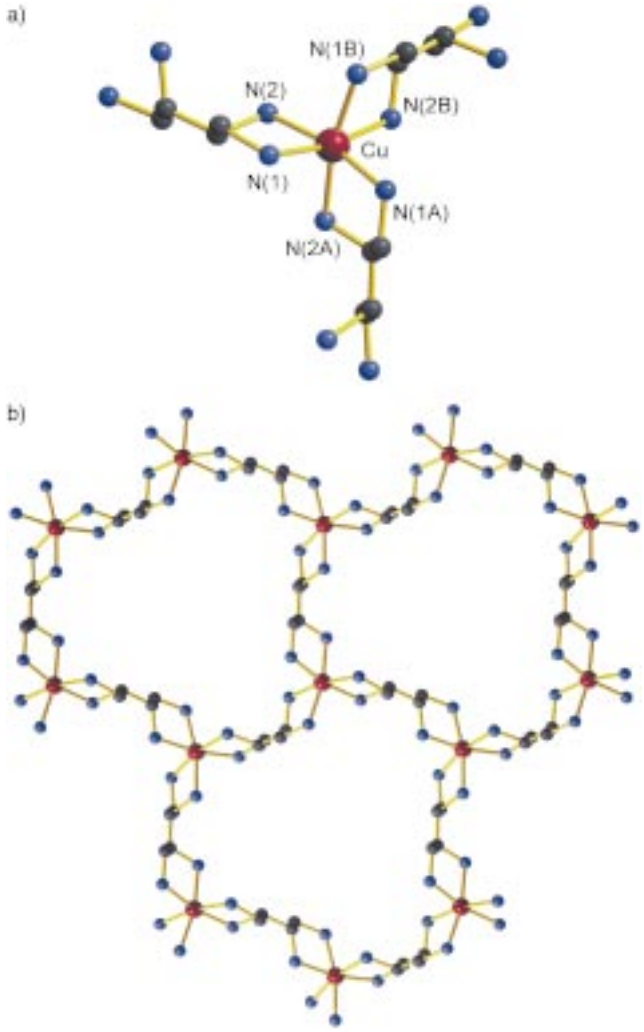

Figure 4. Crystal structure of $Cu_2(ttab)_3Br_4$ (ball and stick model). a) The $[CuL_3]^{2+}$ entity; b) section of the two-dimensional sheet structure (hydrogen atoms omitted). Selected bond lengths [Å] and angles [°]: Cu–N(1) 2.13(2), Cu–N(2) 2.18(1), N(1)-Cu-N(1A) 92.3(5), N(1)-Cu-N(2) 80.3(5), N(1)-Cu-N(2A) 97.3(6), N(1)-Cu-N(2B) 168.1(6), N(2)-Cu-N(2A) 91.3(5).

-symmetric Cu_2L unit with a bis-bidentate (1,2)-(3,4)-coordinating ligand in common (Figure S3, Supporting Information). In $Cu_2(ttab)_3Br_4$, however, each Cu center is coordinated to three ligands and the resulting tris-chelate has crystallographically imposed C_3 symmetry with a $\Delta(\lambda\lambda\lambda)$ conformation (Figure 4a). Of the four different possible forms, this conformation has been reported to have the lowest energy.[13] The combination of the (1,2)-(3,4)-bis-bidentate binding mode of the ligand together with the tris-

0947-6539/01/0704-0920 $ 17.50+.50/0 *Chem. Eur. J.* **2001**, *7*, No. 4

chelated Cu^{II} centers generates an infinite two-dimensional honeycomb-type sheet structure of fused, puckered Cu_6L_6 rings (Figure 4b). The crystallographic C_3 axes go through the Cu^{II} centers and through the midpoints of the Cu_6L_6 rings, while the C_2 axes go through the midpoints of the C(2)–C(3) bonds of the tetraamine ligands. The entire structure can finally be described as a stack of such chiral trigonal sheets along the *c* axis; these sheets are staggered in that the Cu cations of one sheet are placed above the centers of the Cu_6L_6 rings of the adjacent sheet and vice versa. With regard to the Cu positions, the fused Cu_6L_6 rings have an ideal chair form with Cu-Cu-Cu angles of 110° and a *trans*-decalin-type linking (Figure S4, Supporting Information). This type of arrangement is closely related to the rhombohedral modification of the Group 15 elements P (high-pressure modification), As, Sb, and Bi, in which the atomic positions E correspond to the Cu positions and the E–E bonds have to be replaced by the bis-bidentate tetraamine ligands.[14] However, since this ligand is chiral, all the improper elements of symmetry are no longer operative. As a consequence, the Group 15 elements crystallize in the centrosymmetric space group $R\bar{3}m$, whereas $Cu_2(t\text{tab})_3Br_4$ crystallizes in the acentric space group *R*32. It is worth noting that *R*32 represents one of the maximal non-isomorphic subgroups of $R\bar{3}m$, in which all proper elements of symmetry are retained.[15] In this sense, the structure of $Cu_2(t\text{tab})_3Br_4$ may be regarded as a chiral analogue of the rhombohedral Group 15 element structure. In the rhombohedral modification of the Group 15 elements every atom has three nearest neighbors (the directly bonded atoms) at a distance r_1 and in addition three neighbors in the next layer at a somewhat greater distance r_2. In accord with metallic behavior increasing in the order P, As, Sb, Bi the ratio r_2:r_1 decreases (1.53, 1.25, 1.154, and 1.149, respectively).[14] For $Cu_2(t\text{tab})_3Br_4$ r_1 is 7.07 Å and r_2 is 8.00 Å, giving a ratio r_2:r_1 of only 1.13, and with regard to a specific Cu atom the six neighboring Cu atomic positions form an almost regular octahedron. The two Br^- counter ions do not have any direct interaction with the Cu^{II} centers. They are both disordered and have partial occupancies. Br(2) is placed in proximity to a threefold axis and is distributed over three crystallographically equivalent sites, whereas Br(1) is located in proximity to a twofold axis and is distributed over two crystallographically equivalent sites. This disorder problem is probably the reason for the somewhat high value of the *R* index of 7.5 %.

An even more pronounced disorder was found in the Ni^{II} complex $[Ni_8(t\text{tab})_{12}]Br_{16}\cdot 17.5\,H_2O$ (Figure 5). In this compound, an octanuclear $[Ni_8(t\text{tab})_{12}]^{16+}$ cube could be located and refined without problems. However, the Br^- counter ions and several water molecules proved to be severely disordered. Numerous attempts to grow crystals of better quality by using a variety of different counter anions proved unsuccessful. These problems prevented a satisfactory crystal structure analysis as indicated by the final *R* index of 10.9 %. The structure determination was, however, sufficient to establish unambiguously the connectivity of the $[Ni_8(t\text{tab})_{12}]^{16+}$ cube. All bond lengths and angles within this molecule fall in expected ranges,[16] and the structure is consistent with a chemically sensible model. Owing to the rather interesting properties of this molecule, we will discuss the connectivity of this cluster here although the structural analysis cannot be considered complete.

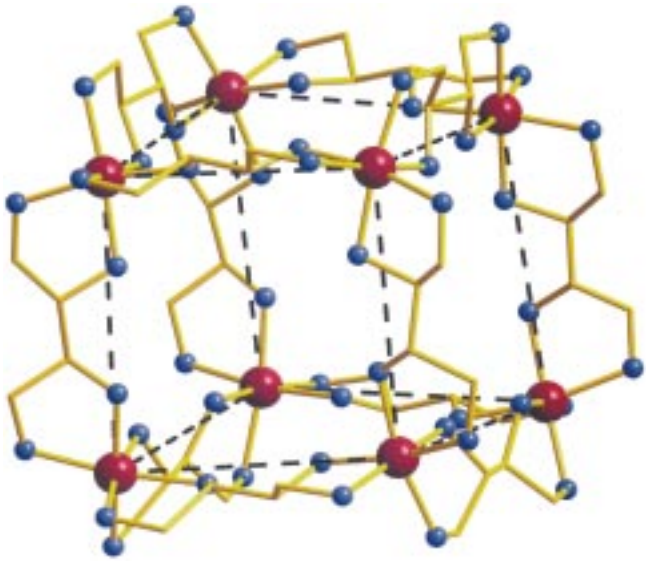

Figure 5. Molecular structure of the $[Ni_8(t\text{tab})_{12}]^{16+}$ cube (ball and stick model). The Ni–N bond lengths fall in the range of 2.08(2)–2.19(2) Å.

$[Ni_8(t\text{tab})_{12}]Br_{16}\cdot 17.5\,H_2O$ has the same metal-to-ligand ratio as the above-described rhombohedral Cu complex. However, in contrast to this Cu complex, which forms an infinite layered structure, the Ni^{II} complex consists of discrete octanuclear molecules (Figure 5). The eight Ni centers are located on the vertices of a slightly distorted cube. The edges of the cube are occupied by the twelve tetraamine ligands, which exhibit a similar bis-bidentate (1,2)-(3,4) coordination as already observed for the two Cu complexes. However, the conformations of the ligands in the Ni complex on the one hand and in the Cu complexes on the other show characteristic differences. In the Ni complex the two chelate rings of a ligand are approximately coplanar, whereas in the Cu complexes they are tilted by an angle of about 60°. This difference corresponds to an internal rotation around the C(2)-C(3) bond as expressed by the value for the torsional angle C(1)-C(2)-C(3)-C(4), which is about 180° for the two Cu complexes but 66–74° for the Ni complex. As in $Cu_2(t\text{tab})_3Br_4$, each Ni center is coordinated to three ligands and exhibits distorted octahedral NiN_6 coordination. The eight Ni centers have alternating Λ or Δ configuration, and the Ni_8 cube can be subdivided into two interpenetrating tetrahedra in which all four Ni centers either have Δ or Λ configuration. Due to the uniform chirality of the twelve ligand molecules, the complex thus represents a chiral cube, adopting, approximately, the rather rare tetrahedral *T* symmetry.[17] The entire structure can be described as an alternating stack of layers of Ni_8 cubes. In each layer the cubes are arranged in such a way that they form columns along the two face diagonals of the *ab* plane (Figure S5, Supporting Information). The volume of each cube is sufficient to accommodate additional molecules such as H_2O or some of the Br^- counter ions. However, it seems that the cavity of the cube is too large for these entities and consequently they showed considerable disorder. Sim-

ilarly, some of the counter ions and water molecules that were located between the cuboidal complex molecules are disordered and are distributed over several sites with partial occupancy. It was not possible to resolve the disorder problem and to localize the Br^- counter ions or water molecules unambiguously. Evidently, the unsatisfactorily high R index is due to the relatively large amount of electron density which is represented by these disordered moieties.

Speciation in dilute aqueous solution: The tetraamine ligands *t*tab and *e*tab are both tetravalent bases and can be isolated as the fully protonated tetraammonium cations H_4*t*tab^{4+} and H_4*e*tab^{4+}, respectively.[8] Values for the pK_a for the chiral H_4*t*tab^{4+} are listed in Table 1. For comparison, the previously determined values of the achiral H_4*e*tab^{4+} are also shown. Evidently, the acidity constants of the two diastereomers are the same within experimental error. In the presence of Ni^{II} or Cu^{II}, a large number of different metal complexes $[M_xL_yH_z]^{(2x+z)+}$ are formed in dilute aqueous solution, and an unambiguous elucidation of their composition, structure, and stability has proved difficult. Moreover, the partially protonated $[Cu(H_2$*t*tab$)]^{4+}$ is of such high stability that the use of excess Cu or excess ligand resulted in almost complete (>80%) complex formation even at acidic conditions (pH 3). Consequently, in such solutions, the formation constant of this species cannot be determined. Moreover, some of the species, such as $[\{ML\}_n]^{2n+}$ and $[M(HL)_2]^{4+}$, are formed in the same pH range (Figure 6, and Figures S6, S7, and S8 in the Supporting Information), and the unambiguous evaluation of a single titration curve is therefore not possible because the corresponding formation constants are highly correlated; it is easily possible to increase the value of one constant at the cost of the other. One must also keep in mind that titration experiments only provide information about the overall composition x,y,z of a so called macrospecies $[M_xL_yH_z]^{(2x+z)+}$. However, as shown in Scheme 2, for many of these macro species a variety of different microspecies must be considered. This problem has already been encountered when considering the large number of isomers found for $[Co(H$*e*tab$)_2]^{5+}$.

We used a multiple step procedure to shed light on the species composition in aqueous solutions. In a first step, a series of pH titration experiments was carried out with a large excess of the metal. As shown for the Cu^{II}–*t*tab system (Figure 6c) this system is relatively simple and comprises mainly free Cu^{2+}_{aq}, the protonated 1:1 complex $[CuLH_2]^{4+}$ at the beginning, and the dinuclear $[Cu_2L]^{4+}$ at the end of the titration. Since each of these species dominated clearly at different pH ranges, it was possible to determine the equilibrium constant for the reaction $[CuLH_2]^{4+} + Cu^{2+} \rightleftharpoons [Cu_2L]^{4+} + 2H^+$ unambiguously. In the next step, solutions with a large excess of ligand were investigated. This allowed the direct determination of a series of formation constants for the 1:2 complexes $[CuL_2H_x]^{(2+x)+}$ starting from $[CuLH_2]^{4+}$. Titrations with a Cu:L ratio of 1:1 were then evaluated by using the previously determined equilibrium constants as

Table 1. pK_a values[a-c] of the tetraammonium cations H_4*e*tab^{4+} and H_4*t*tab^{4+} (25 °C, 0.1 mol dm^{-3} KCl).

	H_4*e*tab^{4+}	H_4*t*tab^{4+}
pK_1	1.4(1)	1.5(1)
pK_2	5.03	5.02
pK_3	8.40	8.41
pK_4	9.65	9.66

[a] $pK_i = -\log K_i$; $K_i = [H_{4-i}L][H][H_{5-i}L]^{-1}$. [b] The estimated standard deviations are 0.01 or less unless otherwise noted. [c] The data for H_4*e*tab^{4+} are from ref. [8].

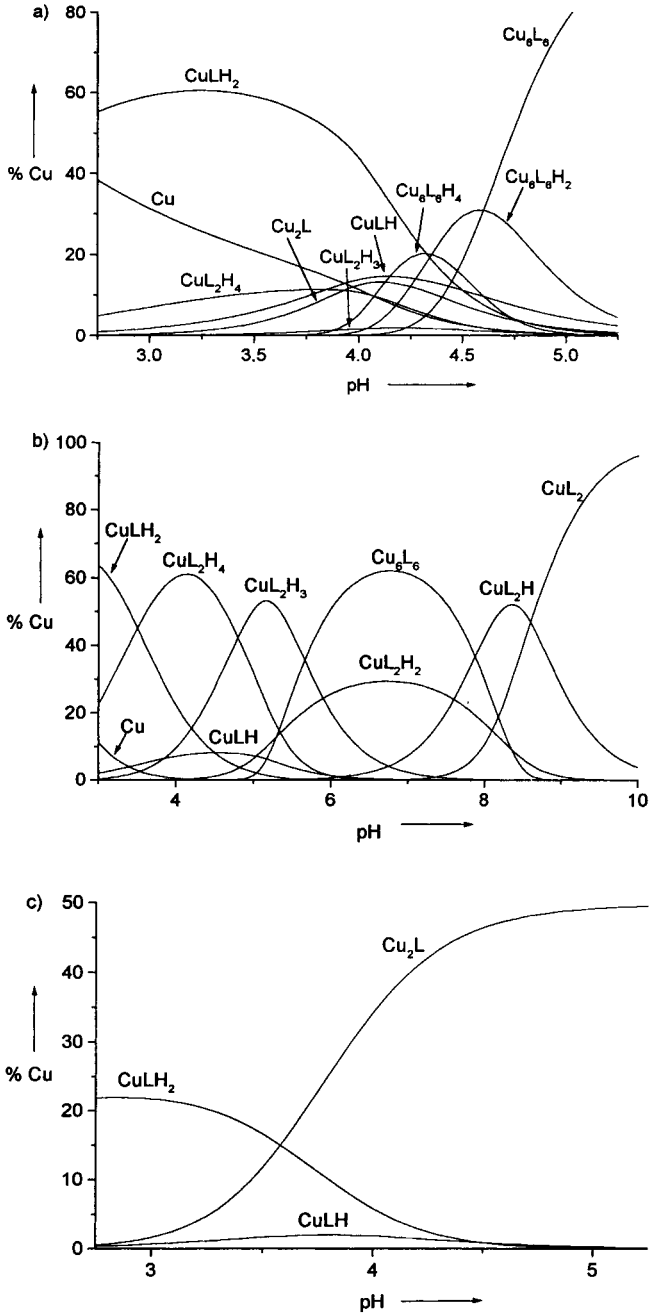

Figure 6. pH-dependent species distribution plot for the Cu^{II}-*t*tab system. The distributions were calculated using the formation constants listed in Tables 1 and 2. a) Equimolar concentrations of Cu and L (10^{-3} mol dm^{-3}); b) excess ligand (total L = 10^{-3} mol dm^{-3}, total Cu = 2.5×10^{-4} mol dm^{-3}); c) excess Cu (total L = 10^{-3} mol dm^{-3}, total Cu = 4×10^{-3} mol dm^{-3}, the free Cu^{2+} which is here present in excess over the entire pH range is not shown).

0947-6539/01/0704-0922 $ 17.50+.50/0 *Chem. Eur. J.* **2001**, *7*, No. 4

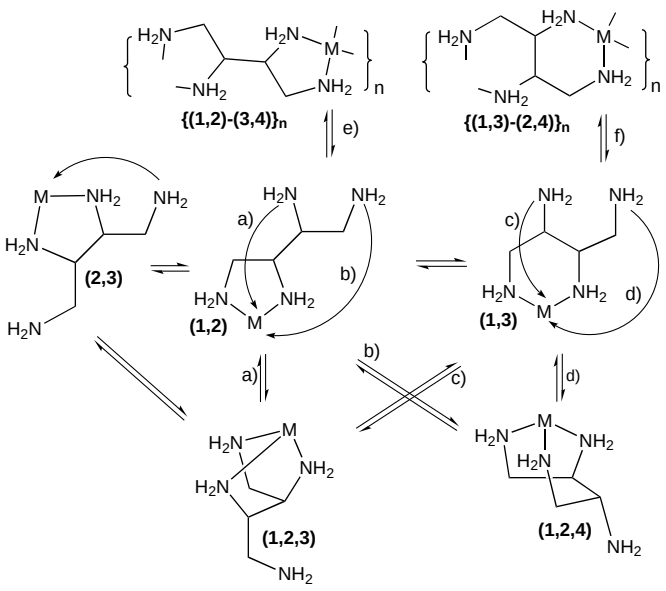

Scheme 2. Equilibrium between different microspecies of composition $[ML]^{2+}$ (a–d) and the polymeric $[ML]_n^{2n+}$ (e, f).

fixed values. The resulting constants for the 1:1 complexes were then imported as fixed values for a re-evaluation of the titration curves with excess ligand or excess metal. This procedure was repeated until one consistent model was obtained for the entire data set. Finally multiple titration curves with different total concentrations (total metal: 0.12–4.05 mmol dm^{-3}, total ligand: 0.10–1.00 mmol dm^{-3}) or different M:L ratios (1:4, 1:2, 1:1, 4:1) were evaluated simultaneously to consolidate the model. Altogether, the entire data set that was used in the final evaluation was composed of a total of 28 different titration curves. An analogous procedure was used for the Cu^{II}-*e*tab, Ni^{II}-*t*tab, and Ni^{II}-*e*tab systems (Table 2).

For Ni–*e*tab, the titration data could be fitted with high accuracy to the derived model, whereas for Ni–*t*tab, Cu–*e*tab, and Cu–*t*tab, the fit was remarkably poor, particularly for the M:L = 1:1 titrations. However, the fit could be significantly improved by the consideration of polynuclear species $[(ML)_n]^{2n+}$ (Figure 7). Therefore, in a subsequent refinement, some of the mononuclear 1:1 complexes were replaced by corresponding polynuclear species, and the nuclearity *n* was systematically increased until an optimal fit was obtained.

Table 2. Formation constants[a] $\log\beta_{xyz}$ for $[M_xL_yH_z]^{(2x+z)+}$ complexes with L = *e*tab, *t*tab and M = Ni^{II}, Cu^{II} (25.0 °C, 0.1 mol dm^{-3} KCl).

	*e*tab		*t*tab	
xyz	Ni	Cu	Ni	Cu
110	10.5(1)			
111	18.0(1)	19.4(1)	17.4(1)	19.5(1)
112		23.5(1)	21.9(1)	24.0(1)
120	19.1(1)	20.5(1)	18.5(1)	19.9(1)
121	27.3(1)	29.0(1)	26.4(1)	28.5(1)
122	35.0(1)	37.0(1)	33.8(1)	36.1(1)
123		41.8(2)	38.8(2)	42.0(1)
124				46.8(1)
660				109.2(1)
662				118.4(1)
664				127.1(1)
330		52.5(1)		
220			24.0(1)	
221		38.6(1)		
210	13.8(1)	19.4(1)	13.7(1)	19.1(1)

[a] $\beta_{xyz} = [M_xL_yH_z][M]^{-x}[L]^{-y}[H]^{-z}$.

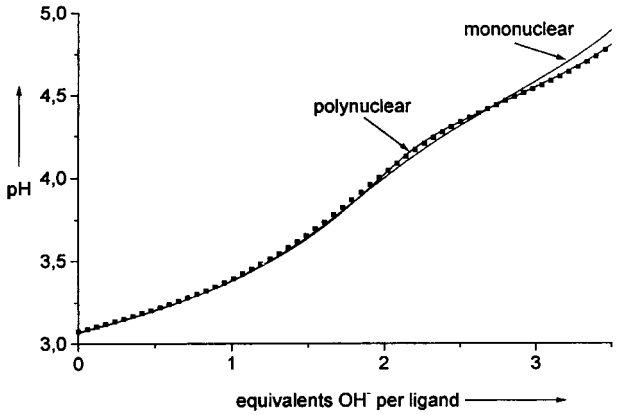

Figure 7. Observed and calculated titration curves for a the Cu^{II}–*t*tab system (total L = total Cu = 5×10^{-4} mol dm^{-3}). The simulated curves are shown as solid lines and correspond to the best fit model comprising only mononuclear species or hexanuclear species as listed in Table 2.

In a third step, the potentiometric data of the Cu^{II}–*t*tab system was supplemented with spectrophotometric measurements. For this purpose, the titration cell was equipped with an immersion probe for UV/Vis detection (diode array spectrophotometer), and a spectrum was recorded automatically prior to each addition of the titrant (Figure 8 and Figure S9). Evaluation of the resulting series of spectra confirmed the final model derived from the potentiometric measurements. The formation constants obtained by the two different methods were in close agreement and any differences generally fell within the range expected on the basis of the estimated standard deviations. Moreover this method allowed the calculation of the spectra for all the individual species and provided valuable information for a structural assignment. It is well known that in aqueous solution, Cu^{II}–amine complexes exhibit absorption in the range of 500–700 nm. Although it has been pointed out that depending on the geometry of the coordination sphere more than one transition is to be expected for the d^9 configuration,[18] usually only a single broad band is observed at 25 °C in solution.[19] It is also well known that for a tetragonally distorted octahedral complex, successive replacement of the four aqua ligands in the equatorial plane by nitrogen donors results in a continuous shift of the observed transition to shorter wavelengths, whereas the replacement of the axially, loosely bound water ligands by nitrogen donors results in a red shift ("pentaammine effect").[20, 21] Hathaway has demonstrated that the spectral properties of polycrystalline Cu^{II} amine complexes can be used as a diagnostic tool to get information on the nature of the coordination sphere.[22] Similar considerations are also possible for solution samples. We performed a comprehensive search for solution spectra of Cu^{II} complexes with saturated polyamines with sp^3-nitrogen donors or water

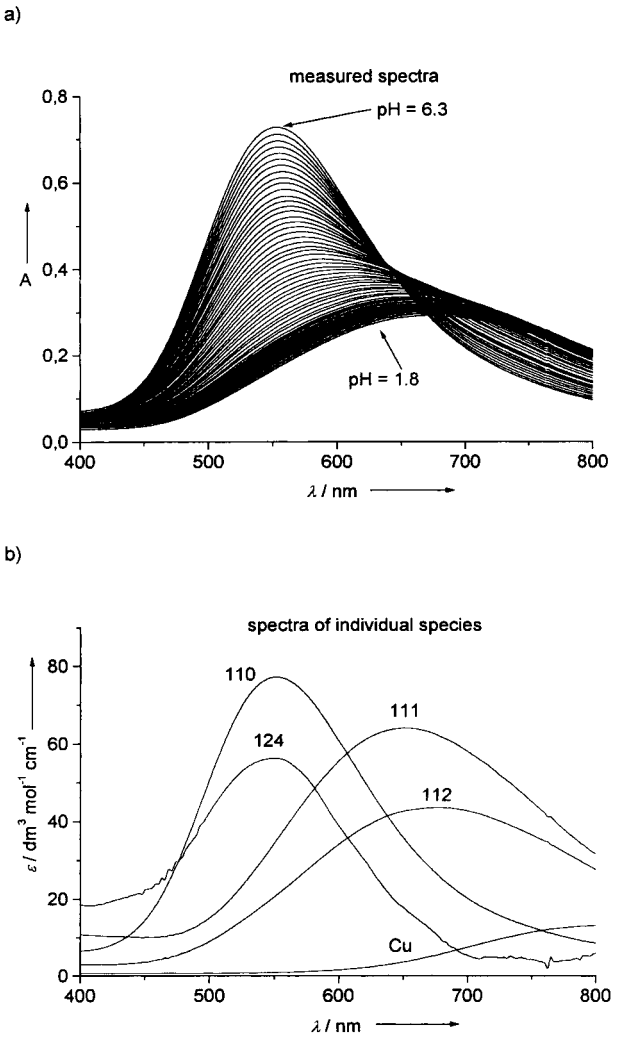

Figure 8. a) Spectral changes for the Cu^{II}–*t*tab system during a titration experiment with total Cu = total L = 10^{-2} mol dm^{-3}; b) the calculated spectra for the individual species of composition $Cu_xL_yH_z$ (labeled as *xyz*).

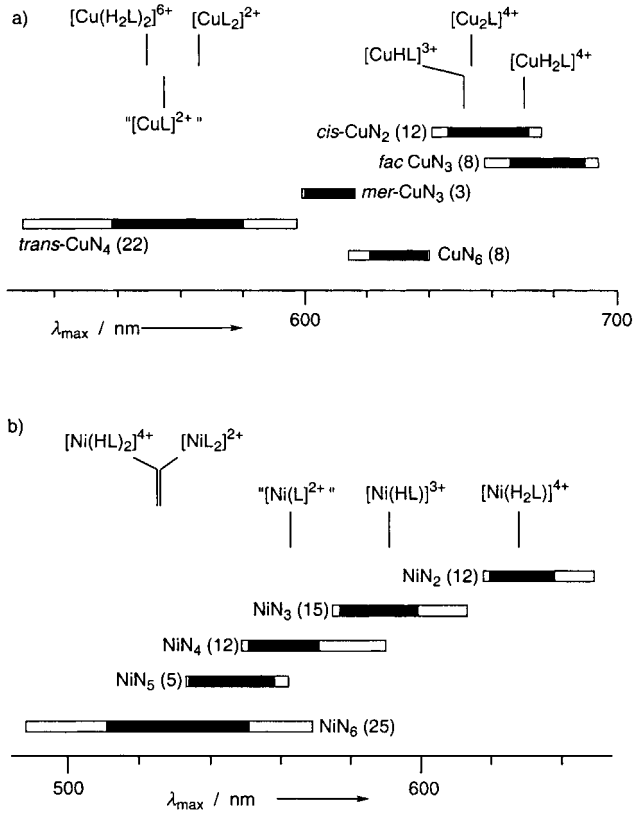

Figure 9. Survey of λ_{max} for the visible spectra of a) Cu^{II}– and b) Ni^{II}–amine complexes in aqueous solution. Only complexes with H_2O and with amines with sp^3-nitrogen donors (aliphatic and alicyclic polyamines) as ligands are considered. Literature data[23] of λ_{max} [Ni: $^3A_{2g}$-$^3T_{1g}(F)$ transition] is shown for different chromophores as indicated. The number of references for each chromophore is given in parentheses. Open boxes refer to the entire range reported, black boxes represent the averages ± one standard deviation. The data are compared with λ_{max} observed for the L = *t*tab complexes investigated in this study.

as the only ligands.[23] A graphical representation of this search together with the spectral properties of some of the Cu-*t*tab complexes is shown in Figure 9a. $[Cu(H_2L)_2]^{6+}$ exhibits maximal absorbance at about 550 nm. This value is clearly indicative of a square-planar (*trans*) CuN_4 chromophore with one or two weakly bound water molecules at the apices. A tentative structure could be a bis-(2,3) coordination mode (Scheme 2) with both ligands having protonated amino groups in the 1- and 4-position. It is interesting to note that the successive deprotonation to $[CuL_2]^{2+}$ does not result in a significant shift of λ_{max}. Evidently, a pentaammine effect is not operative, and we can therefore exclude a tridentate (1,2,3)- or (1,2,4)-coordination mode even for the completely deprotonated ligands. For $[CuLH_2]^{4+}$ λ_{max} is about 670 nm. This value is consistent with a *cis*-CuN_2 chromophore, and we tentatively assign a (2,3)-structure to this species as well, based on electrostatic arguments and by analogy with the crystal structure of the corresponding Pd complex. After deprotonation of the two amino groups a tridentate coordination mode would now become accessible. However, the spectroscopic data are again in clear contradiction of such a coordination mode. Because of the particular steric constraints of these tetraamine ligands, meridional coordination can be excluded. Facial coordination should, however, result in a red shift similar to the pentaammine effect (Figure 9a). We observe a similar λ_{max} for $[CuLH]^{3+}$ as for $[CuLH_2]^{4+}$ and a dramatic shift to *shorter* wavelength (more than 100 nm) for "$[CuL]^{2+}$". Evidently, $[CuLH]^{3+}$ retains its *cis*-CuN_2 structure with bidentate coordination, whereas the dramatic shift to about 550 nm for "$[CuL]^{2+}$" can only be explained by a square-planar CuN_4 structure of the type already assigned to the bis-complexes. Once more, considering the steric constraints of the tetraamine ligands, such a structure can only be realized in the form of a polymeric species ($\{(1,2)$-$(3,4)\}_n$ or $\{(1,3)$-$(2,4)\}_n$ in Scheme 2). As discussed in the previous section the best model for fitting the potentiometric data of the Cu–*t*tab system comprises the hexanuclear $[Cu_6L_6]^{12+}$ unit as the main species with a Cu:L ratio of 1:1. A tentative structure for such a species is shown in Scheme 3. It must, of course, be emphasized that it is not really possible to establish such a complicated equilibrium system unambiguously. Although the goodness of fit is best for $[Cu_6L_6]^{12+}$, a model with a pentanuclear $[Cu_5L_5]^{10+}$ or heptanuclear $[Cu_7L_7]^{14+}$ gives

0947-6539/01/0704-0924 $ 17.50+.50/0 *Chem. Eur. J.* **2001**, *7*, No. 4

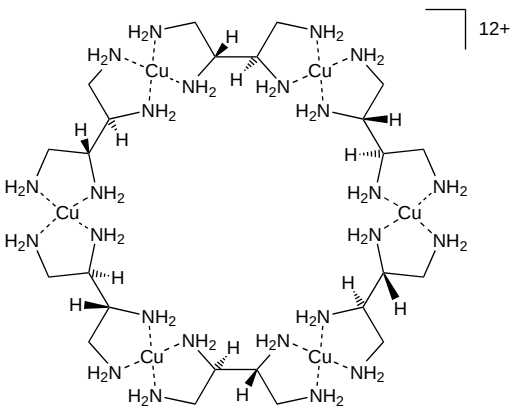

Scheme 3. Tentative structure (based on spectroscopic data, elemental analysis and potentiometric data) for the hexanuclear Cu^{II}–*t*tab complex.

almost the same result, and it seems reasonable that several such polymeric aggregates could well coexist in solution. The hexanuclear $[Cu_6L_6]^{12+}$ should therefore rather be regarded as a representative for small ($4 < n < 10$) oligonuclear species. However, the potentiometric data together with the spectrophotometric measurements are a clear indication that the amount of the mononuclear $[CuL]^{2+}$ ($n = 1$) is negligible even in dilute aqueous solution.

A similar comparison of the spectral properties of Ni^{II}–*t*tab complexes with literature data of octahedrally coordinated Ni^{II} complexes with an $\{NiN_x(OH_2)_{6-x}\}$ coordination sphere are shown in Figure 9b. Due to their low intensity ($\log \varepsilon < 1$), the d–d bands of the Ni^{II} complexes are only observable in fairly concentrated solutions ($\geqslant 0.1$ mol dm^{-3}). Corresponding spectra were, therefore, recorded for individual sample solutions, in which the pH was adjusted to such a value that a clear predominance of one species was achieved, and consequently we cannot correlate the UV/Vis results directly with the potentiometric measurements. This is of particular significance for polymeric species, since the degree of polymerization will be strongly dependent upon the sample concentration. Of the three spin-allowed d–d transitions of an octahedral (high-spin) Ni^{II}–amine complex we focused on the $^3A_{2g} - {}^3T_{1g}(F)$ transition, which has an absorbance maximum in the range of 490–700 nm.[24] This transition is usually readily detected and shows a characteristic increase with increasing number x of coordinated nitrogen donors in the chromophore. Although the ranges for different x show a considerable overlap (Figure 9b), the differences for the individual chromophores are sufficiently large to draw the following conclusions: $[Ni(HL)_2]^{4+}$ and its deprotonation products $[NiL(HL)]^{3+}$ and $[NiL_2]^{2+}$ all show an absorbance maximum at about 525 nm and, therefore, adopt the same hexaamine coordination. This is in contrast to the Cu^{II} system in which tetraamine coordination was observed for the bis-complexes. It appears though that similarly to Co^{III}, the bis-complexes of Ni^{II} are mononuclear with a bis-(1,2,3)-, bis-(1,2,4)- or a mixed (1,2,3)-(1,2,4)-coordination mode with the additional possibility for protonation of the non-coordinating amino group. Moreover, the close agreement of the spectral data for these species with $[Ni(trap)_2]^{2+}$ (trap = 1,2,3-triaminopropane) points to a bis-(1,2,3)-type structure with formation of two five-membered chelate rings.[25] Note that Ni^{II} hexaamine complexes with six-membered chelate rings appear at the low-energy end of the range observed for hexaamine complexes.[20, 26] An other interesting result is the steady shift to shorter wavelength in the series $[Ni(H_2ttab)]^{4+}$ (628 nm), $[Ni(Httab)]^{3+}$ (592 nm), and $[Ni(ttab)]^{2+}$ (563 nm). The observed wavelengths for $[Ni(H_2ttab)]^{4+}$ and $[Ni(Httab)]^{3+}$ fit well with the expected NiN_2 and NiN_3 chromophore.[23] However, the observed absorbance of $[Ni(ttab)]^{2+}$ at 563 nm can only be explained by the coordination of at least four nitrogen donors, and, as in $[Cu(ttab)]^{2+}$, this complex must have a polymeric-$\{(1,2)$-$(3,4)\}_n$ or -$\{(1,3)$-$(2,4)\}_n$ structure (Scheme 2).

Discussion

Our solution study has clearly shown that in terms of formation of different macrospecies $[M_xL_yH_z]^{(2x+z)+}$, in the cases of Cu^{2+} and Ni^{2+} relatively simple systems are only observed either for sufficient excess of metal or sufficient excess of ligand. For the intermediate range (0.5 < total M:total L < 2) these systems become exceedingly complicated owing to the formation of polymeric aggregates. Even in case of excess M or L, the assignment of a molecular structure to the individual complexes (i.e., the identification of microspecies) proved at best difficult or even impossible. We therefore carried out a variety of molecular mechanics (MM) calculations to elucidate the relative energies of the different isomers (Table 3). These results will be discussed here together with the spectral properties, the stability constants of the solution species, and the solid state structures to gain further insight into the molecular architecture of tetraaminobutane-complexes. The MM calculations were mainly per-

Table 3. Strain energies [kJ mol^{-1}] and distribution ratios for the different isomers of $[Co(etab)_2]^{3+}$ according to molecular mechanics calculations.

diastereomer[a]	conformation	ΣU	abundance [%][b]
bis-(1,2,3)			
cis-trans-cis	$\lambda\delta$, $\lambda\delta$	85.2	8.9
trans-trans-trans	$\lambda\delta$, $\lambda\delta$	85.3	8.8
cis-cis-trans	$\lambda\delta$, $\lambda\delta$	85.9	6.8
cis-cis-cis	$\lambda\delta$, $\lambda\delta$	85.9	6.7
trans-cis-cis	$\lambda\delta$, $\lambda\delta$	85.2	8.9
bis(1,2,4)			
cis-trans-cis	chair, chair	87.5	3.5
trans-trans-trans	chair, chair	92.4	0.5
cis-cis-cis	chair, chair	88.3	2.6
cis-cis-trans	chair, chair	87.9	3.1
trans-cis-cis	chair, chair	85.4	8.4
(1,2,3)-(1,2,4)			
cis-trans-cis	chair, $\lambda\delta$	86.3	5.7
trans-trans-trans	chair, $\lambda\delta$	86.5	5.3
cis-cis-cis	chair, $\lambda\delta$	86.3	5.9
cis-cis-trans	chair, $\lambda\delta$	86.3	5.8
trans-cis-cis	chair, $\lambda\delta$	85.8	7.2
*cis-cis-cis**	chair, $\lambda\delta$	86.2	6.0

[a] For nomenclature, see Scheme 1. [b] 16 additional high-energy species with a bis-(1,2,4) or a mixed (1,2,3)-(1,2,4) structure and a twisted boat conformation of the six-membered ring have an abundance of < 1%. The total amount of these species accounts for the remaining 5.9%.

formed with Co^{III}–hexaamine models, since the available force field for this system is well established,[27] and it has been shown that the structure and energy of Co–hexaamine complexes can be predicted with good accuracy for a broad range of examples with different polyamine ligands.[28]

Complex formation in the presence of excess ligand: In sufficiently acidic solutions, in which the tetraamine ligands are mainly protonated (H_4L^{4+} and H_3L^{3+}), the doubly protonated $[M(H_2L)]^{4+}$ complexes (L = *t*tab: M = Ni, Cu; L = *e*tab: M = Cu) are formed upon addition of a metal salt. $[Ni(H_2etab)]^{4+}$ seems not to be of sufficient stability to tolerate the high electrostatic repulsion caused by the 4+ charge. Progressive increase of the pH leads to an increasing amount of free ligand, which allows the coordination of a second ligand and subsequent deprotonation of the coordinated H_xL. This leads to a series of bis-complexes [Eq. (1)]:

$$[M(H_2L)_2]^{6+} \xrightarrow{pK_1} [M(HL)(H_2L)]^{5+} \xrightarrow{pK_2} [M(HL)_2]^{4+} \xrightarrow{pK_3} [M(L)(HL)]^{3+} \xrightarrow{pK_4} [ML_2]^{2+} \quad (1)$$

Only the Cu–*t*tab system is of sufficient stability to allow significant formation of the fully protonated $[M(H_2L)_2]^{6+}$. For the other systems this species is not observed, most probably because the high positive charge causes electrostatic destabilization. Consistent with the non-observance of $[Ni(H_2etab)]^{4+}$, there is no evidence for the formation of the triply protonated $[Ni(HL)(H_2L)]^{5+}$. A survey of the overall stability constants (Table 2) shows the following general trends:

1) Comparison of corresponding Ni and Cu complexes $[ML_2H_x]^{(2+x)+}$ of the same ligand L, we note that for $x = 0$ there is only a minor preference for Cu ($\Delta\log\beta = \log\beta_{Cu} - \log\beta_{Ni} = 1.4$). This behavior is remarkable as aliphatic polyamines usually show a much more pronounced affinity for Cu^{II}.[29] It can be explained in terms of the tridentate and bidentate coordination for Ni and Cu, respectively. Evidently, the intrinsically higher stability of the Cu^{II} complex is almost completely compensated by the higher denticity of L in the Ni complex. With increasing x, $\Delta\log\beta$ increases steadily. Since the doubly protonated ligand must of course coordinate in a bidentate fashion in both cases, $[Cu(Htab)(H_2ttab)]^{5+}$ is, as expected, significantly more stable than $[Ni(Httab)(H_2ttab)]^{5+}$ (the value $\Delta\log\beta = 3.2$ is almost identical with the difference observed for $[Cu(en)]^{2+}$ and $[Ni(en)]^{2+}$). It is also interesting to compare the evaluated formation constants with those of 1,2-diaminoethane (en) and 1,2,3-triaminopropane (trap). $[Ni(trap)_2]^{2+}$ is considerably more stable than $[Ni(en)_2]^{2+}$, whereas $[Ni(trap)_2]^{2+}$ and $[Ni(tab)_2]^{2+}$ are of similar stability (Table 4). This trend clearly shows a significant stabilization of the Ni complex by the tridentate coordination of the tri- or tetraamines. In contrast $[Cu(en)_2]^{2+}$, $[Cu(trap)_2]^{2+}$, and $[Cu(tab)_2]^{2+}$ all have about equal stability, which once again points to bidentate coordination of all four ligands.

2) Complexes with the same metal but different ligands show very similar stability for the diastereomeric *e*tab and *t*tab. It seems that in the species $[ML_2H_x]^{(2+x)+}$ with $x \leqslant 2$, the *e*tab derivatives are slightly more stable. This is in contrast to complexes with $x \geqslant 3$ for which either the *e*tab complex is less stable or does not form at all.

Table 4. Comparison of the overall formation constants $\log\beta(ML_2)$[a] for different linear polyamine ligands.[b]

	en	2,2-tri	trap	*t*tab	*e*tab
NiL_2	13.4	18.6	17.4	18.5	19.1
CuL_2	19.6	20.9	19.6	19.9	20.5

[a] $\beta(ML_2) = [ML_2][M]^{-1}[L]^{-2}$. [b] en: 1,2-diaminoethane, 2,2-tri: 1,4,7-triazaheptane (both ref. [32]); trap: 1,2,3-triaminopropane (ref. [8]); *e*tab and *t*tab: *erythro*- and *threo*-1,2,3,4-tetraaminobutane (this work).

3) Trends in the pK_a values: for the inert $[Co(Hetab)_2]^{5+}$, $pK_3 = 6.31(1)$ and $pK_4 = 7.01(1)$ could be determined directly. They are assignable to the all-*trans*-bis(1,2,3) isomer as identified by crystal structure analysis. For $[CuH_4(ttab)_2]^{6+}$ ($pK_1 = 4.8$, $pK_2 = 5.9$, $pK_3 = 7.6$, $pK_4 = 8.6$), $[NiH_3(ttab)_2]^{5+}$ ($pK_2 = 5.0$, $pK_3 = 7.4$, $pK_4 = 7.9$), $[CuH_3(etab)_2]^{5+}$ ($pK_2 = 4.8$, $pK_3 = 8.0$, $pK_4 = 8.5$) and $[NiH_2(etab)_2]^{4+}$ ($pK_3 = 7.7$, $pK_4 = 8.2$) corresponding values could be calculated from the overall stability constants (Table 2); they refer to an average of all the different microspecies.[30] We note that with respect to Co^{III}, the corresponding complexes of the divalent cations are slightly weaker acids, as would be expected. The triply protonated $[Cu(Hetab)(H_2etab)]^{5+}$ is a considerably stronger acid than $[Cu(Httab)(H_2ttab)]^{5+}$, whereas for the less protonated species the reverse order is observed. Finally, for the same ligand, the Ni^{II} complexes are generally more acidic than the corresponding Cu^{II} complexes. As already discussed in 1) above, this is a consequence of different denticity, and the measured "pK_2" value of $[NiH_3(ttab)_2]^{5+}$ refers to a two-step reaction consisting of deprotonation and N–Ni bond formation. Tridentate coordination of L and HL in the bis-complexes of Ni^{II} and corresponding bidentate coordination of Cu^{II} is indicated, therefore, not only by the spectroscopic properties, but it can also be deduced from a careful analysis of stability constants.

Our preparative work with Co^{III} showed that in the presence of excess ligand a variety of different isomeric hexaamine complexes are formed. For the ligand *e*tab, a total of 16 different isomers must to be taken into account (Scheme 1) with either a different binding mode ((1,2,3) or (1,2,4) coordination) or a different spatial orientation of the two ligands (*cis*–*trans* isomerism). Moreover, different forms with a λ or δ conformation (five-membered chelate rings) or a chair or boat conformation (six-membered chelate rings) must also be considered. Conformational flexibility is of particular significance for the (1,2,4)-coordination mode, which is considerably more flexible than the relatively rigid (1,2,3) mode. For a total of 32 different geometries of $[Co(etab)_2]^{3+}$, energy-minimized structures were calculated by using MM methods (Table 3), and an isomer distribution based on the difference in strain energy and statistical effects (entropic stabilization) was then deduced.[27] These calculations showed the predominance of 12 species, each with an abundance of 5–9%. Three additional species appear to the extent of 2–4%. The rest corresponds to high energy

0947-6539/01/0704-0926 $ 17.50+.50/0 *Chem. Eur. J.* **2001**, *7*, No. 4

structures each with less than 1% abundance. The calculations showed that the (1,2,3) mode with two five-membered chelate rings predominates slightly. All five isomers with this mode correspond to low-energy species. However, there are also some species with a mixed (1,2,3)-(1,2,4) structure of only minimally higher energy. The bis-(1,2,4) mode with five-, six-, and seven-membered chelate rings seems to be less favored, and there is only one low-energy species with this structure. Three additional isomers of this type appear with about 2–4% abundance (to be compared with 9% abundance of the most stable species). Hence, it seems evident that the difference in energy for several of these species is rather small, and considering the limited accuracy of this method it is not really possible to predict whether the (1,2,3) or (1,2,4) structure would be more favorable in such a bis-complex. If one regards solid-state phases, additional intermolecular interactions based on the anion–cation packing will also contribute to the overall energy and must be taken into account. Nevertheless, it is noteworthy that the isomer in the crystalline $[Co(Hetab)_2][ZnCl_4]_2Cl \cdot H_2O$ does indeed correspond to one of the three species of lowest energy.

For bis-bidentate coordination as observed in $[CuL_2]^{2+}$ with its *trans*-CuN_4 chromophore, the situation is less complex. Bidentate coordination of one tetraamine ligand gives rise to two structures with a five-membered chelate ring (1,2) or (2,3), one structure with a six-membered chelate ring (1,3) and one structure with a seven-membered chelate ring (1,4). The last structure is of very high energy and will not be considered. Calculations for hexaamine Co^{III} complexes (in which the remaining axial coordination sites were occupied by NH_3 ligands) exhibited lowest energy for five-membered ring structures. Although difference in energies for such isomers is rather small for both tetraamine ligands the structure with a bis-(2,3) mode seems to be favored.

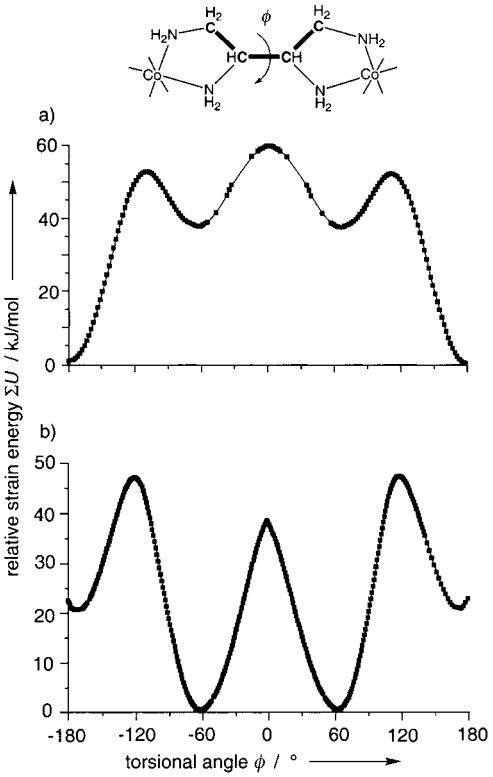

Figure 10. Overall strain energy ΣU ($kJ\,mol^{-1}$) as a function of the torsional angle ϕ calculated by molecular mechanics methods for a) $[(H_3N)_4Co^{III}$-*e*tab-$Co^{III}(NH_3)_4]^{6+}$ and b) $[(H_3N)_4Co^{III}$-*t*tab-$Co^{III}(NH_3)_4]^{6+}$.

Complex formation in the presence of excess metal: The behavior of this system is particularly simple. As above, a mononuclear, partially protonated 1:1 complex $[MLH_2]^{4+}$ or (in the case of Ni–*e*tab) $[MLH]^{3+}$ is formed in sufficiently acidic solution. However, with the addition of base, these species are converted to the binuclear $[M_2L]^{4+}$ (Figure 6c). It is noteworthy that protonation products are generally not observed in the case of dinuclear species. Evidently, $[M_2L]^{4+}$ has a similar bis-bidentate coordination as that observed in the corresponding solid-state structures of the Cu^{II} and Ni^{II} complexes. Two different structures must be considered for such species: a (1,2)-(3,4) mode with two five-membered chelate rings or a (1,3)-(2,4) structure with two six-membered chelate rings (due to the very unfavorable energy, a (1,4)-(2,3) coordination with a seven- and five-membered chelate ring is again excluded from further consideration). MM calculations were performed for a hypothetical $[(H_3N)_4Co^{III}$-L-$Co^{III}(NH_3)_4]^{6+}$ (L = *e*tab or *t*tab) complex to elucidate the amount of strain in the two different coordination modes. The (1,2)-(3,4)-mode exhibits considerable conformational flexibility due to possible rotation around the C(2)–C(3) single bond (Figure 10). The strain energy was analyzed as a function of the C(1)-C(2)-C(3)-C(4) torsional angle ϕ, which exhibits minima for $\phi = 60^\circ$ and 180° and maxima for $\phi = 0^\circ$ and 120°. The two diastereomeric tetraamines showed some characteristic differences. The $\phi = 60^\circ$ form represents a global minimum for the *threo* isomer, but only a local minimum for the *erythro* isomer, whereas the converse holds for $\phi = 180^\circ$. These findings can easily be explained in terms of a maximization of the number of staggered orientations for the non-hydrogen substituents at the C(2)–C(3) bonds for lowest energy. It is worth noting that in the solid-state structures of $[Ni_8(ttab)_{12}]Br_{16} \cdot 17.5\,H_2O$, $[Cu_2(ttab)Br_4] \cdot H_2O$ and $Cu_2(ttab)_3Br_4$, the Ni complex adopts the lowest energy conformation ($\phi = 66–74^\circ$), while the two Cu complexes correspond to the somewhat less stable $\phi = 180^\circ$ structure. In this particular case the $\phi = 180^\circ$ structure was evidently stabilized by N–H···O···H–N hydrogen bonds. No evidence has yet been found for a (1,3)-(2,4)-coordination mode with two six-membered chelate rings. This mode would correspond to the rather rigid decalin-structure with a *cis*-decalin geometry for the *threo*, and a *trans*-decalin geometry for the *erythro* isomer. MM calculations showed that for both ligands the decalin-type $[(H_3N)_4Co^{III}$-L-$Co^{III}(NH_3)_4]^{6+}$ structure is of higher energy and that the (1,2)-(3,4) mode would be favored. This is due, in particular, to unfavorable non-bonding interactions between an axial NH_3 ligand and the axial C(3) or C(4) hydrogen atoms. However, as expected for *trans*-decalin, the (1,3)-(2,4) structure of the *erythro* isomer is less destabilized. The difference in energy for the most stable conformers of the (1,2)-(3,4) and the (1,3)-(2,4) mode is

20 kJ mol^{-1} for the *threo* isomer, but only 14 kJ mol^{-1} for the *erythro* isomer. If the octahedral Co^{III} center were to be replaced by a metal cation with a square-planar coordination geometry, further release of strain could be expected, and, at least for the *erythro* isomer, the (1,3)-(2,4) mode could well be formed.

Complex formation for 0.5 < M:L < 2: Acidic solutions of this composition also contain the mononuclear, partially protonated 1:1 complex. As discussed above, a doubly protonated $[Ni(H_2etab)]^{4+}$ is not observed, and the first step of complex formation of this system involves the monoprotonated $[Ni(Hetab)]^{3+}$. For all other systems the doubly protonated species is well established. According to MM calculations, the lowest energy for a $[M(H_2L)]^{4+}$ complex should be observed for the (2,3) structure with the two protonated nitrogens in the 1- and 4-positions. The Pd^{II} complex found in $[Pd(H_2ttab)Cl_2]Cl_2 \cdot H_2O$ is an illustrative example of this mode. Abstraction of one proton leads to $[M(HL)]^{3+}$. According to the spectroscopic data, the Ni^{II} and Cu^{II} complexes of this type are still mononuclear and adopt either tridentate (Ni) or bidentate (Cu) coordination. For $[CuLH]^{3+}$, we expect a change to a (1,2) structure with the remaining proton on N(4) (maximal distance between the two positive charges). According to MM calculations carried out on the hypothetical mononuclear $[Cu(ttab)]^{2+}$, the final step of this deprotonation sequence would return to the (2,3) structure. We note, however, (and this is probably the most important result of this paper) that such an $[ML]^{2+}$ complex, carrying two additional free amino groups, has capacity for further metal binding and could easily form polymeric aggregates. It seems that a *mononuclear* $[M(ttab)]^{2+}$ complex is not stable even in dilute (10^{-3} mol dm^{-3}) aqueous solution. This is also true for the Cu – *e*tab systems, although the potentiometric data provided evidence that the tendency of the *erythro* isomer to form polymeric aggregates is somewhat diminished. The lowest tendency for polymerization was observed for the Ni – *e*tab system. The potentiometric data of a solution of Ni – *e*tab (10^{-3} mol dm^{-3}) could be fitted well by taking only mononuclear species into consideration (models with polynuclear species gave less satisfactory results).

A summary of experimental evidence for the formation of polynuclear species $[\{ML\}_n]^{2n+}$ ($n > 1$) for the Cu – *t*tab, Cu – *e*tab,and Ni – *t*tab systems follows:

1) The potentiometric measurements showed that models of only mononuclear species gave a significantly poorer fit than those which invoked also polynuclear complexes.

2) The spectroscopic data for Ni – *t*tab indicate successive coordination of two, three, and four nitrogen donors to the metal center in the series $[Ni(H_2ttab)]^{4+}$, $[Ni(Httab)]^{3+}$, and $[Ni(ttab)]^{2+}$, respectively. For the last species, two separate ligand entities must be coordinated to one Ni center and, in addition, two metal cations must be bound to each ligand to achieve the 1:1 stoichiometry. Similarly the spectral data for $[Cu(ttab)]^{2+}$ show the presence of a tetragonally elongated *trans*-$CuN_4(OH_2)_x$-chromophore and, therefore, indicate the presence of a polymer.

3) $[Pd(H_2ttab)Cl_2]^{2+}$ proved to be unstable in aqueous solution. A freshly prepared solution of $[Pd(H_2ttab)Cl_2]Cl_2 \cdot H_2O$ showed a slow but steady drop in pH until a value was reached that corresponded to the complete dissociation of the two protons. Because the ammonium groups in an $[MH_xL]^{(2+x)+}$ complex generally behave as weak acids, the complete release of the protons must be interpreted as the substitution of the chloro ligands by amino groups, that is, $\cdots Pd^{II}$-L-Pd^{II}-L-$Pd^{II} \cdots$ formation.

d) The crystal structures of $[Ni_8(ttab)_{12}]Br_{16} \cdot 17.5\,H_2O$ and $Cu_2(ttab)_3Br_4$ indicate either a discrete octanuclear complex (Ni) or an infinite two-dimensional network (Cu) for complexes with a ligand to metal ratio of 1.5:1. We have not yet succeeded in isolating a macrocrystalline compound with an exact M:L = 1:1 composition. However, in the titration of a solution of $Cu(NO_3)_2/H_4ttab^{4+}$ (0.01 mol dm^{-3}; 25 °C, 1 mol dm^{-3} KNO_3) we observed the quantitative precipitation of a purple, microcrystalline solid after addition of 4.0 equiv of KOH. The analysis for this solid indicated the composition $\{Cu(ttab)(NO_3)_2\} \cdot 2\,H_2O$, and the diffuse reflectance spectrum had an absorption maximum at 550 nm. Again, the maximum below 600 nm is only consistent with a *trans*-CuN_4O_x chromophore and, therefore, with a polymeric structure (Scheme 3).

Conclusion

The results presented in this paper clearly confirmed our contentions outlined in the previous contribution of this series,[8] that linear polyamines of composition H_2N-CH_2-$(CH$-$NH_2)_n$-CH_2-NH_2 with more than three NH_2 groups ($n \geqslant 2$) are powerful, potential chiral building blocks for coordination polymers. Our investigation provides evidence that polymeric aggregates are not only formed in the solid state, but are also present in dilute aqueous solution. Two different strategies have been presented in this paper for the construction of such polynuclear species:

1) The use of high metal to ligand ratios leads to the exclusive formation of the $[M_2L]^{4+}$ cation. This species can be regarded as a chiral cationic building block, which can be packed together with a suitable inorganic anion to form an organic – inorganic hybrid material. $[Cu_2(ttab)Br_4] \cdot H_2O$ is a typical representative of such compounds.

2) If the metal and ligand are employed in comparable amounts, each ligand molecule will bind to more than one metal ion and each metal ion will coordinate to more than one ligand. The consequence of this interlinking is either the formation of discrete polynuclear species or aggregation, giving rise to multidimensional infinite networks. In either case, the chiral nature of the ligand will lead to a chiral structure. Examples: $[Ni_8(ttab)_{12}]Br_{16} \cdot 17.5\,H_2O$, $Cu_2(ttab)_3Br_4$.

The bis-bidentate-(1,2)-(3,4) coordination has been shown to be the basic structural motif in both cases 1) and 2). The conformational flexibility of this mode (rotation around the C(2)–C(3) bond) is an important structure-determining factor as can be seen by comparing the ϕ angles for $[Ni_8(ttab)_{12}]Br_{16} \cdot 17.5\,H_2O$ (66 – 74°) and $Cu_2(ttab)_3Br_4$ (180°).

0947-6539/01/0704-0928 $ 17.50+.50/0 *Chem. Eur. J.* **2001**, *7*, No. 4

Experimental Section

Safety note: Organic polyazides are highly explosive. They should only be handled in dilute solutions and should not be isolated as pure substances.

Materials: Metal salts that were used for the potentiometric titrations were of highest possible quality (from Fluka). All other chemicals were commercially available products of reagent-grade and were used without further purification. Dowex 50WX2 (100–200 mesh, H^+ form) and Dowex 2-X8 (50–100 mesh, Cl^- form) were purchased from Fluka. The OH^- form of the anion resin was obtained from the Cl^- form by elution with 0.3 mol dm^{-3} NaOH, followed by extended rinsing with CO_2-free water until a neutral eluent was observed. SP-Sephadex C-25 (200 mesh) cation-exchange resin was from Pharmacia Biotech.

NMR spectroscopy and analyses: ^{1}H and ^{13}C NMR spectra were measured in D_2O or $CDCl_3$ on a Bruker DRX500 NMR spectrometer. Chemical shifts (in ppm) are given relative to sodium (trimethylsilyl)propionate (D_2O) or tetramethylsilane ($CDCl_3$) as internal standard ($\delta = 0$). Concentrated solutions of NaOD and DCl in D_2O were used for pD adjustment. C, H, and N analyses were performed by H. Feuerhake (Universität des Saarlandes).

UV/Vis spectra: Single spectra of solution samples (H_2O) were measured on a Uvikon 941 spectrophotometer ($25 \pm 3\,^\circ$C). The collection of a pH-dependent series of spectra (Figure 8 and Figure S9) of the Cu^{II}–*t*tab complexes was performed by equipping a titration cell (50 mL sample solution, 0.01 mol dm^{-3} total Cu, 1 mol dm^{-3} KNO_3, $25.0 \pm 0.1\,^\circ$C) with an immersion probe (HELLMA), which was connected to a diode array spectrophotometer (J&M, TIDAS-UV/NIR/100–1). A home-built computer program was used to control the addition of the titrant (1 mol dm^{-3} KOH). This program allowed registration of a sample spectrum prior to each addition of an increment of titrant. The diffuse reflectance spectrum of the solid $\{Cu(ttab)(NO_3)_2\} \cdot 2H_2O$ was measured on a UV/Vis-NIR Lambda 19 (Perkin Elmer) spectrophotometer.

Potentiometric measurements: Potentiometric titrations were carried out with a Metrohm 713 pH/mV-meter and a Metrohm combined glass electrode with an internal Ag/AgCl reference. The sample solutions (50 mL) were titrated with KOH (0.1 mol dm^{-3}), by means of a Metrohm 665 piston burette. The stability of the electrode was checked by a calibration titration prior to, and after, each measurement. All titrations were performed at $25.0 \pm 0.1\,^\circ$C under nitrogen (scrubbed with an aqueous solution of 0.1 mol dm^{-3} KCl) at an ionic strength of 0.1 mol dm^{-3} (KCl). For the pK_a determination of H_4ttab^{4+} and of $[Co(Hetab)_2]^{5+}$, several alkalimetric titrations were carried out with analytically pure samples of $ttab \cdot 4HCl \cdot 0.75H_2O$ or of $[Co(Hetab)_2]Cl_5 \cdot 2H_2O$ (total concentrations: 10^{-3} or 5×10^{-4} mol dm^{-3}, respectively). The formation constants of metal complexes were determined by using solutions that contained the tetrahydrochlorides of *e*tab or *t*tab and the metal salt in a 4:1, 2:1, 1:1, and 1:4 molar ratio with total $L = 1.0 \times 10^{-3}$ or 0.5×10^{-3} mol dm^{-3}. The samples were made up by using standardized aqueous stock solutions of $etab \cdot 4HCl$, $ttab \cdot 4HCl$, $CuCl_2 \cdot 2H_2O$, and $NiCl_2 \cdot 6H_2O$. At least three separate titrations were performed for every sample solution. Complete equilibration was always ensured by back titrations, which exhibited no significant hystereses. Further details of the potentiometric measurements and data evaluation are summarized in Tables S2 and S3 (Supporting Information).

Calculations of equilibrium constants: All equilibrium constants were calculated as concentration quotients. Potentiometric titrations were evaluated by using the computer program SUPERQUAD.[31] A value of 13.79 was used for pK_w.[32] The titration experiments of the metal complexes were evaluated with fixed values for the total concentrations of M, L, and H, and for the pK_a's of the ligands (Table 1). The spectrophotometric data of the Cu complexes were evaluated with the computer program SPECFIT.[33, 34]

Ligands: (2*R*,3*S*)-1,2,3,4-Tetraaminobutane · 4HCl was prepared as described previously.[8] The same method was also used for the synthesis of the *threo* isomer (2*S*,3*S*)-1,2,3,4-tetraaminobutane: D-Threitol was converted into the tetrabenzenesulfonate (66%). Elemental analysis calcd (%) for $C_{28}H_{26}O_{12}S_4$ (682.75): C 49.26, H 3.84; found C 49.07, H 3.94; ^{1}H NMR ($CDCl_3$): $\delta = 4.09$–4.10 (m, 4H; CH_2), 4.80 (m, 2H; CH), 7.54–7.82 (m, 20H; aryl-H); ^{13}C NMR: $\delta = 66.1$, 75.0, 128.0, 128.2, 129.5 (2C), 134.4, 134.6, 134.8, 135.0. The tetrabenzenesulfonate was then converted into the tetraazide. ^{1}H NMR ($CDCl_3$): $\delta = 3.57$–3.62 (m, 6H); ^{13}C NMR: $\delta = 51.9$, 61.4. A solution of the tetraazide in EtOH/Et_2O was finally hydrogenated to give the tetraamine, which was isolated as the tetrahydrochloride · $0.75H_2O$ (from Dowex 50). Yield: 62% of a white solid. Elemental analysis calcd (%) for $C_4H_{19.5}Cl_4N_4O_{0.75}$ (277.5): C 17.31, H 7.08, N 20.19; found C 17.46, H 7.16, N 20.03; ^{1}H NMR (D_2O, pD < 2): $\delta = 3.30$–3.35 (2H; CH_2), 3.51–3.54 (2H; CH_2), 3.73–3.77 (2H; CH); ^{1}H NMR (D_2O, pD > 12): $\delta = 2.70$–2.72 (m, 4H), 2.54–2.56 (m, 2H); ^{13}C NMR (pD < 2): $\delta = 42.6$, 53.0; ^{13}C NMR (D_2O, pD > 12): $\delta = 46.0$, 55.5.

$[Co(Hetab)_2][ZnCl_4]_2Cl \cdot H_2O$: An aqueous solution (60 mL) of *e*tab · 4HCl (962 mg, 3.64 mmol) was placed in a two-neck round-bottomed flask and small portions of aqueous NaOH (15%) were added until a pH of 7 was reached. $CoCl_2 \cdot 6H_2O$ (434 mg, 1.82 mmol), dissolved in of H_2O (50 mL), and charcoal (50 mg) was then added. The flask was fitted with a reflux condenser, the mixture was heated to 80 °C for 48 h, and a gentle steady stream of air was passed through the mixture. The charcoal was removed by filtration, the filtrate was acidified with aqueous HCl to a pH of 1.6 and diluted with water to a total volume of 300 mL. This solution was sorbed on Dowex 50, and the column was eluted successively with water, 0.1 mol dm^{-3} HCl and 3 mol dm^{-3} HCl. The last fraction was evaporated to dryness under reduced pressure and the remaining solid (821 mg) was redissolved in water and sorbed onto Sephadex. Elution with 0.2 mol dm^{-3} trisodium citrate gave one broad, orange band which was collected, desalted on Dowex 50, and evaporated to dryness again. Yield 592 mg (1.16 mmol). Crystallization of the resulting solid from 4 mol dm^{-3} aqueous HCl gave a fraction which contained only one single component. ^{1}H NMR (D_2O): $\delta = 2.99$–3.07 (m, 4H), 3.38–3.41 (m, 4H), 3.46–3.48 (m, 2H), 3.58 (m, 2H); ^{13}C NMR (D_2O): $\delta = 40.7$, 43.1, 57.3, 61.9; elemental analysis calcd (%) for $C_8H_{34}Cl_5CoN_8O_2$ (510.61): C 18.82, H 6.71, N 21.95; found C 18.42, H 6.93, N 21.77. Crystals of the tetrachlorozincate salt were obtained by dissolving the complex (6 mg) in a few mL of H_2O and adding a solution of $ZnCl_2$ (124 mg dissolved in 1 mL of 3 mol dm^{-3} HCl). The crystals were redissolved by heating to 60 °C, and slow cooling resulted in the deposition of single crystals which were suitable for the X-ray diffraction study. Elemental analysis calcd (%) for $C_8H_{32}Cl_9CoN_8OZn_2$ (765.15): C 12.56, H 4.22, N 14.64; found C 12.86, H 4.50, N 14.41.

$[Cu_2(ttab)Br_4] \cdot H_2O$: *t*tab · 4HCl (65 mg, 0.246 mmol) was dissolved in water (10 mL) and deprotonated over Dowex 2-X8 (OH^- form). The solution of the free amine (pH 10) was evaporated to dryness under reduced pressure. The oily residue was then redissolved in water (5 mL) and a solution of $CuBr_2 \cdot 2H_2O$ (24.6 mg, 0.111 mmol) in water (5 mL) was added. The resulting turquoise solution was evaporated to a volume of about 3 mL and layered with EtOH. After a few months green crystals, suitable for X-ray diffraction experiments appeared and were collected. Elemental analysis calcd (%) for $C_4H_{16}Br_4Cu_2N_4O$ (582.93): C 8.24, H 2.77, N 9.61; found C 8.48, H 3.04, N 9.42.

$Cu_2(ttab)_3Br_4$: $ttab \cdot 4HCl \cdot 0.75H_2O$ (100 mg, 0.36 mmol) was dissolved in water (10 mL) and deprotonated as described in the previous section. The oily residue was redissolved in water (5 mL) and a solution of $CuBr_2 \cdot 2H_2O$ (36 mg, 0.162 mmol) in water (5 mL) was added. The remaining solution was layered with EtOH yielding a small crop of blue crystals which were suitable for X-ray analysis.

$Ni_8(ttab)_{12}Br_{16} \cdot 17.5H_2O$: $ttab \cdot 4HCl \cdot 0.75H_2O$ (100 mg, 0.36 mmol) was dissolved in water (10 mL) and deprotonated as described above. The oily residue was dissolved in water (5 mL) and a solution of $NiBr_2 \cdot 3H_2O$ (44 mg, 0.162 mmol) in water (5 mL) was added. The solution was layered with EtOH yielding a small crop of tiny pink crystals. Larger crystals could be grown by repeating this procedure and by using the small crystals for seeding. This procedure was repeated several times until a few crystals of acceptable size were obtained.

$[Pd(H_2ttab)Cl_2]Cl_2 \cdot H_2O$: $ttab \cdot 4HCl \cdot 0.75H_2O$ (51 mg, 0.184 mmol), dissolved in water (10 mL), and $PdCl_2$ (16 mg, 0.092 mmol) were refluxed for 3 h. After cooling a few mL of 6 mol dm^{-3} aqueous HCl was added to the clear solution. After about 30 min yellow needles appeared, which were collected and dried in air. Elemental analysis calcd (%) for $C_4H_{18}Cl_4N_4OPd$ (386.43): C 12.43, H 4.70, N 14.50; found C 12.61, H 4.67, N 14.59.

$\{Cu(ttab)(NO_3)_2\} \cdot 2H_2O$: An aqueous solution of KOH (0.4 mL, 1.0 mol dm^{-3}) was added to an aqueous solution (10 mL) of $Cu(NO_3)_2 \cdot 3H_2O$ (0.01 mol dm^{-3}), $ttab \cdot 4HCl$ (0.01 mol dm^{-3}) and KNO_3 (1 mol dm^{-3}). A dark blue microcrystalline product precipitated. This was

isolated by filtration, washed with three portions of cold water (0 °C), and dried in vacuo (10^{-3} bar) at room temperature. Elemental analysis calcd (%) for $C_4H_{18}CuN_6O_8$ (341.76): C 14.06, H 5.31, N 24.59; found C 14.14, H 4.73, N 24.02.

Molecular modeling calculations: These were carried out as described previously[29] by using the commercially available program MOMEC97.[35] A validation of this force field for Co^{III}-hexaamine complexes is given in ref. [28].

Crystal structure determinations:[36] Data were collected on the following diffractometers (graphite-monochromated $Mo_{K\alpha}$ radiation $\lambda = 0.71073$ Å): STOE IPDS (Pd-complex), Siemens P4 ($Cu_2(t\text{tab})_3Br_4$), Nonius Kappa-CCD (Co complex, Ni complex, $Cu_2(t\text{tab})Br_4 \cdot H_2O$). A compilation of the crystallographic data is given in Table 5. The data were collected at ambient temperature (Pd complex) or at 100(2) K (Co, Ni, Cu complexes). Monitoring of standard reflections during data collection indicated no significant crystal decay ($\leqslant 2\%$). All data sets were corrected for Lorentz and polarization effects. A face-indexed, numerical, or a semi-empirical absorption correction was applied to the data of the Co complex, Pd complex, and $Cu_2(t\text{tab})_3Br_4$, respectively. Intensity data of $[Cu_2(t\text{tab})Br_4] \cdot H_2O$ were corrected by using the program MulScanAbs, which is part of the Platon99 program suite.[37] Corresponding transmission coefficients T_{min} and T_{max} are listed in Table 5. All structures were solved by Direct Methods[38] and refined by full-matrix least-squares calculations[39] on F^2. Data quality of $[Ni_8(t\text{tab})_{12}]Br_{16} \cdot 17.5\,H_2O$ was found to be poor for all three measured specimens. A data subshell between 3 and 0.93 Å was used and the structure was solved in the orthorhombic space group $C222$ (No. 21). The octanuclear cation is located on a crystallographic twofold axis and appeared to be quite well defined, but most of the bromide anions and water molecules are disordered, and their positions had to be split. All four Ni positions, 20 of a total of 24 N positions, and the ordered Br and O positions were refined with anisotropic displacement parameters. The remaining non-hydrogen atoms (N12, N14, N44, N53, some of the partially occupied Br and O, all C) were refined isotropically. The non-hydrogen atoms of the Pd, Co, and the two Cu complexes were all refined with anisotropic displacement parameters. The hydrogen atoms bound to C and N of the Co, Ni, and the two Cu complexes were considered by using a riding model and fixed isotropic displacement parameters with $U_{iso} = 1.2 \times U_{eq}$ of the corresponding heavy atom. The hydrogen atomic position of the water molecule of $[Cu_2(t\text{tab})Br_4] \cdot H_2O$ could be located from the difference map and was isotropically refined. All hydrogen atoms of the Pd complex could be located in a difference map. The H(-C) hydrogens were placed at calculated positions (riding model) and refined with variable isotropic displacement parameters. Atomic coordinates and individual U_{iso} values of the H(-N) and H(-O) positions were refined freely.

Acknowledgement

We thank A. Zaschka (Saarbrücken), Prof. Dr. W. S. Sheldrick (Bochum), and Dr. P. Osvath (Melbourne) for support and helpful suggestions. The structure of the Pd complex was measured and solved by Dr. G. J. Reiß (Düsseldorf), the diffuse reflectance spectrum was measured by Dipl.-Chem. A. Tücks and Prof. Dr. H. P. Beck (Saarbrücken). We thank Dr. R. Kappl and Prof. Dr. J. Hüttermann (Homburg-Saar) for additional EPR measurements. Financial Support from the Studienstiftung des deutschen Volkes (D.K.) and the Fonds der Chemischen Industrie (K.H.) is gratefully acknowledged.

[1] Some comprehensive reviews: a) F. Vögtle, *Supramolecular Chemistry*, Wiley, Chichester, **1991**; b) J.-M. Lehn, *Supramolecular Chemistry*, VCH, Weinheim, **1995**; c) H.-J. Schneider, A. Yatsimirsky, *Principles and Methods in Supramolecular Chemistry*, Wiley, Chichester, **2000**; d) L. R. MacGillivray, J. L. Atwood, *Angew. Chem.* **1999**, *111*, 1080; *Angew. Chem. Int. Ed.* **1999**, *38*, 1018; e) S. R. Batten, R. Robson, *Angew. Chem.* **1998**, *110*, 1558; *Angew. Chem. Int. Ed.* **1998**, *37*, 1460; f) R. W. Saalfrank, B. Demleitner, in *Perspectives in Supramolecular Chemistry*, *Vol. 5* (Ed.: J. P. Sauvage), Wiley-VCH, Weinheim, **1999**, pp. 1 – 51.

[2] Selected recent research papers: a) L. Carlucci, G. Ciani, D. M. Proserpio, *Angew. Chem.* **1999**, *111*, 3700; *Angew. Chem. Int. Ed.* **1999**, *38*, 3488; b) T. Soma, H. Yuge, T. Iwamoto, *Angew. Chem.* **1994**, *106*, 1746; *Angew. Chem. Int. Ed. Engl.* **1994**, *33*, 1665; c) H.-P. Wu, C. Janiak, L. Uehlin, P. Klüfers, P. Mayer, *Chem. Commun.* **1998**, 2637.

[3] For a comprehensive review see: a) M. J. Zaworotko, *Chem. Soc. Rev.* **1994**, 283; b) C. B. Aakeröy, K. R. Seddon, *Chem. Soc. Rev.* **1993**, 397;

Table 5. Crystallographic data for $[Co(H\text{etab})_2][ZnCl_4]_2Cl \cdot H_2O$, $[Pd(H_2t\text{tab})Cl_2]Cl_2 \cdot H_2O$, $[Ni_8(t\text{tab})_{12}]Br_{16} \cdot 17.5\,H_2O$, $[Cu_2(t\text{tab})Br_4] \cdot H_2O$, and $Cu_2(t\text{tab})_3Br_4$

	$[Co(H\text{etab})_2][ZnCl_4]_2Cl \cdot H_2O$	$[Pd(H_2t\text{tab})Cl_2]Cl_2 \cdot H_2O$	$[Ni_8(t\text{tab})_{12}]Br_{16} \cdot 17.5\,H_2O$	$[Cu_2(t\text{tab})Br_4] \cdot H_2O$	$Cu_2(t\text{tab})_3Br_4$
formula	$C_8H_{32}Cl_9CoN_8OZn_2$	$C_4H_{18}Cl_4N_4OPd$	$C_{48}H_{203}Br_{16}N_{48}Ni_8O_{17.5}$	$C_4H_{16}Br_4Cu_2N_4O$	$C_6H_{21}Br_2CuN_6$
habitus, color	orange plate	yellow needle	pink prism	green plate	blue prism
M_r	765.14	386.43	3481.82	582.93	400.65
T [K]	100(2)	293(2)	100(2)	100(2)	293(2)
crystal system	monoclinic	orthorhombic	orthorhombic	tetragonal	rhombohedral
space group	$P2_1/c$	$C222_1$	$C222$	$P4_12_12$	$R32$
a [Å]	10.046(1)	11.793(2)	20.893(4)	6.8042(8)	11.587(4)
b [Å]	15.273(2)	15.793(3)	21.945(4)	6.8042(8)	11.587(4)
c [Å]	16.918(3)	6.7700(10)	29.375(5)	29.612(3)	20.037(5)
α, β, γ [°]	90, 92.08(3), 90	90, 90, 90	90, 90, 90	90, 90, 90	90, 90, 120
V [Å^3]	2594.1(6)	1260.9(4)	13468(4)	1371.0(3)	2329.9(14)
Z	4	4	4	4	6
ρ_{calcd} [g cm^{-3}]	1.959	2.036	1.717	2.824	1.713
μ [mm^{-1}]	3.413	2.297	5.903	14.742	6.536
crystal size [mm]	0.80 × 0.14 × 0.02	0.80 × 0.04 × 0.04	0.24 × 0.24 × 0.12	0.10 × 0.10 × 0.02	0.28 × 0.28 × 0.26
θ max [°]	22.50	26.49	22.49	29.99	23.74
transmssion min/max	0.296/0.933	0.878/0.938		0.355/0.723	0.229/0.357
data set	− 11/11, − 18/18, − 19/20	− 14/14; − 19/19, − 8/8	− 22/26, − 23/21, − 31/38	− 4/10, − 10/6, − 26/43	0/11, 0/11, − 22/22
total/unique data	24 471/3389	4620/1277	46802/8587	3260/1952	828/452
observed reflns [$I > 2\sigma(I)$]	1950	1186	6450	1655	308
Flack parameter[40]		− 0.07(6)	0.17(3)	0.05(4)	0.30(13)
parameters	273	91	476	72	54
R, wR_2 [$I > 2\sigma(I)$]	0.059, 0.108	0.022, 0.054	0.109, 0.285	0.049, 0.113	0.075, 0.180
R, wR_2 (all data)	0.127, 0.130	0.023, 0.054	0.148, 0.349	0.062, 0.118	0.111, 0.221
largest difference peak/hole [e Å^3]	0.786/ − 0.906	0.420/ − 0.489	1.990/ − 1.463	1.533/ − 1.109	0.555/ − 0.397
max shift/error	0.001	0.017	0.003	0.003	0.009

c) G. R. Desiraju, *Angew. Chem.* **1995**, *107*, 2541; *Angew. Chem. Int. Ed. Engl.* **1995**, *34*, 2311; d) H. J. Choi, T. S. Lee, M. P. Suh, *Angew. Chem*. **1999**, *111*, 1490 *Angew. Chem. Int. Ed.* **1999**, *38*, 1405.

[4] Some comprehensive reviews: a) C. Piguet, G. Bernardinelli, G. Hopfgartner, *Chem. Rev.* **1997**, *97*, 2005; b) B. Olenyuk, A. Fechtenkötter, P. J. Stang, *J. Chem. Soc. Dalton Trans.* **1998**, 1707; c) P. J. Stang, B. Olenyuk, *Acc. Chem. Res.* **1997**, *30*, 502; d) A. J. Blake, N. R. Champness, P. Hubberstey, W.-S. Li, M. A. Withersby, M. Schröder, *Coord. Chem. Rev.* **1999**, *183*, 117; e) J. A. R. Navarro, B. Lippert, *Coord. Chem. Rev.* **1999**, *185*, 653; f) P. J. Hagrman, D. Hagrman, J. Zubieta, *Angew. Chem.* **1999**, *111*, 2798; *Angew. Chem. Int. Ed.* **1999**, *38*, 2638; g) M. Albrecht, *Angew. Chem.* **1999**, *111*, 3671; *Angew. Chem. Int. Ed*. **1999**, *38*, 3463; R. W. Saalfrank, E. Uller, B. Demleitner, I. Bernt, *Struct. Bonding* **2000**, *96*, 149.

[5] Selected recent research papers: a) P. N. W. Baxter, J.-M. Lehn, B. O. Kneisel, D. Fenske, *Angew. Chem.* **1997**, *109*, 2067; *Angew. Chem. Int. Ed. Engl*. **1997**, *36*, 1978; b) R. W. Saalfrank, R. Harbig, O. Struck, F. Hampel, E. M. Peters, K. Peters, H. G. von Schnering, *Z. Naturforsch. Teil B* **1997**, *52*, 125; c) A. Neels, H. Stoeckli-Evans, A. Escuer, R. Vicente, *Inorg. Chem.* **1995**, *34*, 1946; d) R. W. Saalfrank, I. Bernt, E. Uller, F. Hampel, *Angew. Chem.* **1997**, *109*, 2596; *Angew. Chem. Int. Ed. Engl*. **1997**, *36*, 2482; e) R. W. Saalfrank, S. Trummer, H. Krautscheid, V. Schünemann, A. X. Trautwein, S. Hien, C. Stadler, J. Daub, *Angew. Chem*. **1996**, *108*, 2350; *Angew. Chem. Int. Ed. Engl*. **1996**, *35*, 2206; f) R. W. Saalfrank, N. Löw, F. Hampel, H.-D. Stachel, *Angew. Chem.* **1996**, *108*, 2353; *Angew. Chem. Int. Ed. Engl*. **1996**, *35*, 2209; g) R. W. Saalfrank, N. Löw, S. Kareth, V. Seitz, F. Hampel, D. Stalke, M. Teichert, *Angew. Chem.* **1998**, *110*, 182; *Angew. Chem. Int. Ed.* **1998**, *37*, 172; h) P. Klüfers, P. Mayer, *Acta Crystallogr. Sect. C* **1998** *54*, 722; i) C. B. Aakeröy, A. M. Beatty, D. S. Leinen, *Angew. Chem.* **1999**, *111*, 1932; *Angew. Chem. Int. Ed*. **1999**, *38*, 1815; j) T. Niu, X. Wang, A. J. Jacobson, *Angew. Chem.* **1999**, *111*, 2059; *Angew. Chem. Int. Ed.* **1999**, *38*, 1934.

[6] A. Togni, L. M. Venanzi, *Angew. Chem.* **1994**, *106*, 517; *Angew. Chem. Int. Ed. Engl.* **1994**, *33*, 497.

[7] U. Knof, A. von Zelewsky, *Angew. Chem.* **1999**, *111*, 312; *Angew. Chem. Int. Ed*. **1999**, *38*, 302.

[8] A. Zimmer, I. Müller, G. J. Reiß, A. Caneschi, D. Gatteschi, K. Hegetschweiler, *Eur. J. Inorg. Chem.* **1998**, 2079.

[9] G. J. Reiß, A. Zimmer, K. Hegetschweiler, *Acta Crystallogr. Sect. C* **2000**, *56*, 284.

[10] P. Hendry, A. Ludi, *Adv. Inorg. Chem.* **1990**, *35*, 117.

[11] F. A. Cotton, G. Wilkinson, *Advanced Inorganic Chemistry*, 5th ed., Wiley, New York, **1988**, pp. 928–929, and references therein.

[12] S. S. Batsanov, *Russ. J. Inorg. Chem.* **1991**, *36*, 1694.

[13] F. A. Cotton, G. Wilkinson, *Advanced Inorganic Chemistry*, 5th ed., Wiley, New York, **1988**, pp. 53–56.

[14] N. Wiberg, *Holleman–Wiberg Lehrbuch der Anorganischen Chemie*, 101th ed., de Gruyter, Berlin **1995**, pp. 794–795, and references therein.

[15] T. Hahn, *International Tables for Crystallography*, *Vol. A*, 4th ed., Kluwer, Dordrecht, **1996**, p. 536.

[16] A. G. Orpen, L. Brammer, F. H. Allen, O. Kennard, D. G. Watson, R. Taylor, *J. Chem. Soc. Dalton Trans.* **1989**, S1.

[17] a) H. Takemura, T. Shinmyozu, T. Inazu, *J. Am. Chem. Soc.* **1991**, *113*, 1323; b) M. Scherer, D. L. Caulder, D. W. Johnson, K. N. Raymond, *Angew. Chem.* **1999**, *111*, 1690; *Angew. Chem. Int. Ed.* **1999**, *38*, 1588; c) R. G. Raptis, I. P. Georgakaki, D. C. R. Hockless, *Angew. Chem.* **1999**, *111*, 1751; *Angew. Chem. Int. Ed.* **1999**, *38*, 1632; d) S. L. James, D. M. P. Mingos, A. J. P. White, D. J. Williams, *Chem. Commun*. **1998**, 2323; e) Y. Miyahara, Y. Tanaka, K. Amimoto, T. Akazawa, T. Sakuragi, H. Kobayashi, K. Kubota, M. Suenaga, H. Koyama, T. Inazu, *Angew. Chem.* **1999**, *111*, 1008; *Angew. Chem. Int. Ed.* **1999**, *38*, 956; f) C. Brückner, R. E. Powers, K. N. Raymond, *Angew. Chem.* **1998**, *110*, 1937; *Angew. Chem. Int. Ed*. **1998**, *37*, 1837; g) D. L. Caulder, R. E. Powers, T. N. Parac, K. N. Raymond, *Angew. Chem*. **1998**, *110*, 1940; *Angew. Chem. Int. Ed*. **1998**, *37*, 1840; h) P. J. Stang, B. Olenyuk, D. C. Muddiman, D. S. Wunschel, R. D. Smith, *Organometallics* **1997**, *16*, 3094; i) M. Nakazaki, K. Naemura, Y. Hokura, *J. Chem. Soc. Chem. Commun.* **1982**, 1245; j) W. D. Hounshell, K. Mislow, *Tetrahedron Lett.* **1979**, 1205; k) R. W. Saalfrank, A. Stark, M. Bremer, H.-U. Hummel, *Angew. Chem*. **1990**, *102*, 292; *Angew. Chem. Int. Ed. Engl*. **1990**, *29*, 311; l) R. W. Saalfrank, B. Hörner, D. Stalke, J. Salbeck, *Angew. Chem*. **1993**, *105*, 1223; *Angew. Chem. Int. Ed. Engl*. **1993**, *32*, 1179.

[18] a) B. J. Hathaway, D. E. Billing, *Coord. Chem. Rev*. **1970**, *5*, 143; b) M. Duggan, N. Ray, B. Hathaway, G. Tomlinson, P. Brint, K. Pelin, *J. Chem. Soc. Dalton Trans.* **1980**, 1342; c) N. J. Ray, L. Hulett, R. Sheahan, B. J. Hathaway *J. Chem. Soc. Dalton Trans.* **1981**, 1463; d) P. Comba, T. W. Hambley, M. A. Hitchman, H. Stratemeier, *Inorg. Chem*. **1995**, *34*, 3903.

[19] a) H. Yokoi, T. Isobe, *Bull. Chem. Soc. Japn*. **1969**, *42*, 2187; b) C. Bianchini, L. Fabbrizzi, P. Paoletti, A. B. P. Lever, *Inorg. Chem.* **1975**, *14*, 197; c) L. Fabbrizzi, P. Paoletti, A. B. P. Lever, *Inorg. Chem*. **1976**, *15*, 1502; d) A. A. Kurganov, V. A. Davankov, *Inorg. Nucl. Chem. Lett.* **1976**, *12*, 743.

[20] C. K. Jorgensen, *Acta Chem. Scand*. **1956**, *10*, 887.

[21] a) J. Bjerrum, B. V. Agarwala, *Acta Chem. Scand*. **1980**, *A34*, 475; b) J. K. Walker, R. Nakon, *Inorg. Chim. Acta* **1981**, *55*, 135; c) H. Sigel, R. B. Martin, *Chem. Rev.* **1982**, *82*, 385.

[22] B. J. Hathaway, *J. Chem. Soc. Dalton Trans.* **1972**, 1196.

[23] A collection of these literature data with references [s1]–[s37] is provided as Supporting Information (Table S1).

[24] A. B. P. Lever, P. Paoletti, L. Fabbrizzi, *Inorg. Chem*. **1979**, *18*, 1324.

[25] G. A. Melson, R. G. Wilkins, *J. Chem. Soc.* **1963**, 2662.

[26] P. V. Bernhardt, P. Comba, *Inorg. Chem.* **1993**, *32*, 2798.

[27] P. Comba, T. W. Hambley, *Molecular Modeling of Inorganic Compounds*, VCH, Weinheim, **1995**.

[28] A. M. T. Bygott, A. M. Sargeson, *Inorg. Chem.* **1998**, *37*, 4795.

[29] J. W. Pauly, J. Sander, D. Kuppert, M. Winter, G. J. Reiß, F. Zürcher, R. Hoffmann, T. F. Fässler, K. Hegetschweiler, *Chem. Eur. J.* **2000**, *6*, 2830.

[30] A. E. Martell, R. J. Motekaitis, *Determination and Use of Stability Constants*, 2nd ed., VCH, New York, **1992**, pp. 75–88.

[31] P. Gans, A. Sabatini, A. Vacca, *J. Chem. Soc. Dalton Trans.* **1985**, 1195.

[32] R. M. Smith, A. E. Martell, R. J. Motekaitis, *Critically Selected Stability Constants of Metal Complexes*, NIST Standard Reference Database 46, Version 5.0, NIST Standard Reference Data, Gaithersburg, MD 20899 (USA), **1998**.

[33] R. A. Binstead, B. Jung, A. D. Zuberbühler, *SPECFIT/32, Version 3.0*, Spectrum Software Associates, Marlborough, MA 01752 (USA), **2000**.

[34] H. Gampp, M. Maeder, C. J. Meyer, A. D. Zuberbühler, *Talanta* **1985**, *32*, 95.

[35] P. Comba, T. W. Hambley, N. Okon, G. Lauer, *MOMEC97, A Molecular Modeling Package for Inorganic Compounds*, Heidelberg **1997**.

[36] Crystallographic data (excluding structure factors) for the structures reported in this paper have been deposited with the Cambridge Crystallographic Data Centre as supplementary publication no. CCDC-148199–CCDC-148203 for $[Co(Hetab)_2][ZnCl_4]_2Cl \cdot H_2O$, $[Pd(H_2ttab)Cl_2]Cl_2 \cdot H_2O$, $[Ni_8(ttab)_{12}]Br_{16} \cdot 17.5\,H_2O$, $[Cu_2(ttab)Br_4] \cdot H_2O$, and $Cu_2(ttab)_3Br_4$, respectively. Copies of the data can be obtained free of charge on application to CCDC, 12 Union Road, Cambridge CB2 1EZ, UK (fax: (+44) 1223-336-033; e-mail: deposit@ccdc.cam.ac.uk)..

[37] A. L. Spek, L. J. Farrugia, *PLATON99 for Windows*, Universities of Utrecht and Glasgow **1999**.

[38] G. M. Sheldrick, SHELXS-86, *Program for Crystal Structure Solution*, Göttingen, **1986**.

[39] G. M. Sheldrick, SHELXL-93, *Program for Crystal Structure Refinement*, Göttingen, **1993**.

[40] H. D. Flack, *Acta Crystallogr. Sect. A* **1983**, *39*, 876.

Received: August 17, 2000 [F2682]